Precambrian Research 170 (2009) 129–156

Contents lists available at ScienceDirect

Precambrian Research

journal homepage: www.elsevier.com/locate/precamres

Cryogenian slate-carbonate sequences of the Tambien Group, Northern Ethiopia (I): Pre-"Sturtian" chemostratigraphy and regional correlations

Nathan R. Miller[a,*], Robert J. Stern[b], Dov Avigad[c], Michael Beyth[d], Bettina Schilman[d]

[a] Department of Geological Sciences, University of Texas at Austin, 1 University Station C1100, Austin, TX 78712-0254, USA
[b] Geosciences Department, University of Texas at Dallas, Box 830688, Richardson, TX 75083-0688, USA
[c] Institute of Earth Sciences, Hebrew University of Jerusalem, Jerusalem 91904, Israel
[d] Geological Survey of Israel, Jerusalem, Jerusalem 95501, Israel

ARTICLE INFO

Article history:
Received 24 July 2007
Received in revised form 2 December 2008
Accepted 31 December 2008

Keywords:
Ethiopia
Snowball Earth Hypothesis
Neoproterozoic
Cryogenian
Sturtian
Sr and C isotope stratigraphy

ABSTRACT

Ethiopia's youngest Neoproterozoic sedimentary outcrops are "Sturtian" diamictites that cap the Tambien Group (Tigre, N. Ethiopia), a modestly thick (1–3 km) slate and carbonate succession that records early Cryogenian evolution of the Mozambique Ocean within the southern Arabian–Nubian Shield. Tambien carbonate deposition occurred over an island arc accretion complex, during or after the waning phase of arc magmatism (Tsaliet Group; ~775–740 Ma) and ended prior to the structural and magmatic emergence of the East African Orogen (EAO; *c.* ≥630–610). Closure of the Mozambique Ocean to form the EAO, sometime after the deposition of "Sturtian" (~715–685 Ma) diamictite and before the onset of EAO magmatism, destroyed accommodation space capable of preserving younger Cryogenian episodes. Litho- and chemostratigraphic variations of the Tambien Group, compiled from investigations of four areas of Tigre, demonstrate that integrated $\delta^{13}C_{carb}$ and $^{87}Sr/^{86}Sr$ stratigraphies are effective for regional correlation and form the basis for a composite reference section (introduced here, but evaluated in the context of evolving Cryogenian Earth systems in a companion manuscript). Sediments in the Negash synclinorium span the depositional histories of all other localities but may contain a significant unconformity, suggesting at least local structural relief differentiation during deposition of the early Tambien Group carbonate platform. Mai Kenetal synclinorium sediments may preserve this missing interval. The regional Tambien record has two consecutive positive-to-negative carbon isotope excursions, the first associated with an abrupt transition to carbonates with cap carbonate-like features (basal Assem Limestone - Mai Kenetal) and the second associated with the transition from relatively organic-rich black limestone to "Sturtian" diamictite (Negash). Sr isotope compositions rise from <0.7055 in dolomites near the base of the carbonate sequence to a stratigraphic plateau near 0.7068 in upper black limestones, before declining to 0.7064 (or lower) in the transition to diamictite deposition. Sr contents of limestones increase (9x) systematically above the lower negative $\delta^{13}C_{carb}$ interval. Textural and chemical properties of the Assem Limestone and its depositional context, suggest a transgressive cap-carbonate sequence. Although conformably underlain by laminated slate without definitive evidence of glaciation, its lithostratigraphic position as the lowest significant carbonate unit correlates regionally above polymict volcaniclastic agglomerates and greywackes (Negash and Samre synclinoria) previously interpreted to have a possible glacigenic origin. Chemical weathering indices (PIA: 92–99) in thick (0.5–1.1 km) slate comprising the lower Tambien Group indicate the Tsaliet arc accretion complex underwent protracted and intensive silicate weathering prior to carbonate deposition. These findings raise the possibility that the initial negative $\delta^{13}C_{carb}$ interval of the Tambien Group corresponds to recovery from an earlier pre-"Sturtian" cooling event, perhaps related to the Kaigas glacial interval. If so, the Assem Limestone is the first and oldest cap carbonate sequence in the Arabian–Nubian Shield. The chemostratigraphic framework for the Tambien Group contributes to empirical observations that integrated C and Sr isotope stratigraphies are effective for Cryogenian (pre-"Sturtian") chemostratigraphic correlations. However, more work is required to understand how $\delta^{13}C_{carb}$ specifically relates to marine $\delta^{13}C_{DIC}$.

* Corresponding author. Tel.: +1 512 471 4810; fax: +1 512 471 9425.
E-mail address: nrmiller@mail.utexas.edu (N.R. Miller).

0301-9268/$ – see front matter © 2009 Elsevier B.V. All rights reserved.
doi:10.1016/j.precamres.2008.12.004

1. Introduction

The Neoproterozoic Era sedimentary record preserves abundant evidence of glaciations between *c.* 760 and 580 Ma, some with low-latitude paleomagnetic inclinations, suggesting that several widespread – even global – icehouse fluctuations of Earth's climate state occurred prior to the first appearance of macroscopic, heterotrophic life (*c.* 575 Ma complex metazoans of the Ediacaran biota). This climatically exceptional 180-myr segue to "Phanerozoic Eras" involved significant, but still incompletely understood, modifications to Earth systems, as exemplified by the Snowball Earth Hypothesis (Kirschvink, 1992; Hoffman et al., 1998). These variations include: supercontinent fragmentation (Rodinia), dispersal, and reconstitution (Greater Gondwana or Pannotia); unprecedented but controversial perturbations of the marine carbon cycle (as indicated by carbonate $\delta^{13}C$, with negative $\delta^{13}C$ excursions associated with icehouse states); possible emergence of carbon dioxide over methane as a predominant greenhouse gas (Pavlov et al., 2003); and a substantial increase (or series of increases) in ocean-atmosphere oxygenation, loosely constrained within the Neoproterozoic (*c.* 1000–700 Ma: Arnold et al., 2004; Canfield and Teske, 1996) but high enough by *c.* 575 Ma (perhaps $\geq$15% of present atmospheric levels; Canfield et al., 2007) to meet the metabolic requirements of large metazoans (Knoll, 1992; Knoll and Carroll, 1999).

Deciphering the nature of Neoproterozoic Earth systems and how they interacted to influence climate and ocean-atmosphere chemistry during Cryogenian (850–630 Ma) and Ediacaran (630–542 Ma) Periods is the focus of interdisciplinary research, from which several competing icehouse earth models have emerged (see Fairchild and Kennedy, 2007 for a recent review). It is of particular interest to determine how Neoproterozoic glacial systems began and, in this regard, it is important to recognize that popular conceptions of Cryogenian systems derive substantially from marine pericratonic (Rodinian) rift margin sequences (Eyles and Januszczak, 2004) postdating the earliest ("Kaigas" and "Sturtian") glacial episodes. Improved understanding of the development of Cryogenian systems requires evidence established among well-preserved marine reference sections from a diversity of paleogeographic settings, but considerable challenges remain. Chief among these are constraining the timing and sequence of Earth system fluctuations from variably metamorphosed sediments. Because biostratigraphy is of limited utility for pre-Ediacaran sedimentary strata and high-resolution radiometric dating methods (e.g., U–Pb zircon SHRIMP) depend on the stratal availability of magmatic products, chemostratigraphic approaches are recognized as having practical potential to derive unambiguous correlations among Neoproterozoic marine successions. However, the efficacy of chemostratigraphy is controversial, and the approach warrants critical evaluation for its vital assumptions (Melezhik et al., 2001; Kaufman et al., 2006). Herein, we present such an evaluation for early Cryogenian metasediments of the Tambien Group in N. Ethiopia (Tigre province) within the southern portion of the Arabian–Nubian Shield (ANS, Fig. 1)—a heretofore little studied intra-oceanic setting.

The ANS is an extensive repository of Neoproterozoic juvenile continental crust (Patchett and Chase, 2002) that is superbly exposed over much of NE Africa and western Arabia (Fig. 1A). Within the Neoproterozoic supercontinent cycle, it formed prior to final Gondwana assembly (between 870 Ma and the end of the Precambrian), in association with the closure of a major ocean basin, known as the Mozambique Ocean (Stern, 1994). Subduction to close the Mozambique Ocean generated numerous island arcs, which collided about 800–650 Ma, and early ANS evolution was correspondingly associated with submarine volcanism and marine sedimentation. Northern Ethiopia (Tigre province), in the southern ANS, contains Neoproterozoic metasediments that record the history of plate tectonic, climatic, and biotic events that characterized the Mozambique Ocean realm during this time (Fig. 1B). Marine carbonates of the Tambien Group record this post-magmatic arc sedimentary phase (Avigad et al., 2007), and may correlate with other carbonate units in southern Arabia, Yemen, and eastern Sudan (*i.e.*, extensive carbonates of the Baileteb Group; Stern et al., 1993). Accretion of island arcs and microcontinents and terminal "Pan African" collision between parts of E and W Gondwana at about 600 Ma formed the East African Orogen (Kröner, 2001; Meert, 2003), as recorded by the prominent NNE-SSW structural grain of Neoproterozoic basement exposures throughout the southern ANS (N. Ethiopia). Renewed magmatic activity succeeded the orogenic phase, as indicated by the widespread occurrence of undeformed post-orogenic intrusives (*c.* $\geq$630–610 Ma in the Tigre region, Fig. 1B).

Cryogenian strata with depositional hallmarks of icehouse climate conditions occur in the ANS and "Sturtian" glacigenic deposits are postulated in northern Ethiopia (Tambien Group) from limited geochronological and chemostratigraphic constraints (Miller et al., 2003; Stern et al., 2006; Alene et al., 2006; Avigad et al., 2007). Herein we document the baseline record of Tambien Group lithostratigraphy and chemostratigraphy (principally $\delta^{13}C$ and $^{87}Sr/^{86}Sr$), as established from transects sampled in four areas of Tigre, and evaluate the efficacy of chemostratigraphy for regional correlation. A companion manuscript will integrate age constraints to construct a composite Tambien Group reference section for Tigre, and assess how the Tambien Group may relate to other pre-"Sturtian" sequences and the broader framework of Cryogenian tectonics, marine chemistry, and climate (Miller et al., in prep). These initiatives constitute the first comprehensive investigation of the Tambien Group and how its deposition within the ANS may relate to Cryogenian Earth systems.

2. Geological setting of the Tambien Group

The basic Neoproterozoic stratigraphic framework for northern Ethiopia and Eritrea was established by Beyth (1971, 1972). Key aspects of Tigre's Neoproterozoic basement architecture and stratigraphic organization, including the Tambien Group, were first compiled in the Mekele (1:250,000) sheet map (Arkin et al., 1971). Chief among these observations were identities of major lithologic units, their general thicknesses and contact relations; relationships of metasedimentary units to syn- and post-tectonic intrusives; and recognition that deformed Neoproterozoic basement was unconformably overlain by Paleozoic and Mesozoic rocks (Enticho and Adigrat Sandstones, respectively; Fig. 3).

2.1. Overview of the Tambien Group within the Neoproterozoic basement complex

Low-grade, deformed Neoproterozoic supracrustal successions of Tigre are sporadically preserved in fold-and-fault structures as the Tsaliet Group, an older island arc metavolcanic and slate sequence of unknown thickness, and the overlying Tambien Group, a modestly thick (1–3 km) metasedimentary succession (Fig. 2) of slates and carbonates. The contact between these two groups is poorly understood, ranging from seemingly conformable and gradational to fault-bounded (Sifeta et al., 2005). An unconformable basal contact also was postulated from considerable lateral variations observed among basal Tambien metasediments (Arkin et al., 1971; Beyth, 1972; Tadesse, 1999). Neoproterozoic metavolcanics and metasediments originally accumulated in a complex of marine environments associated with one or more island arc systems. The arc phase produced syn-tectonic intrusives, effusive flows, and diverse volcaniclastics associated with the Tsaliet Group

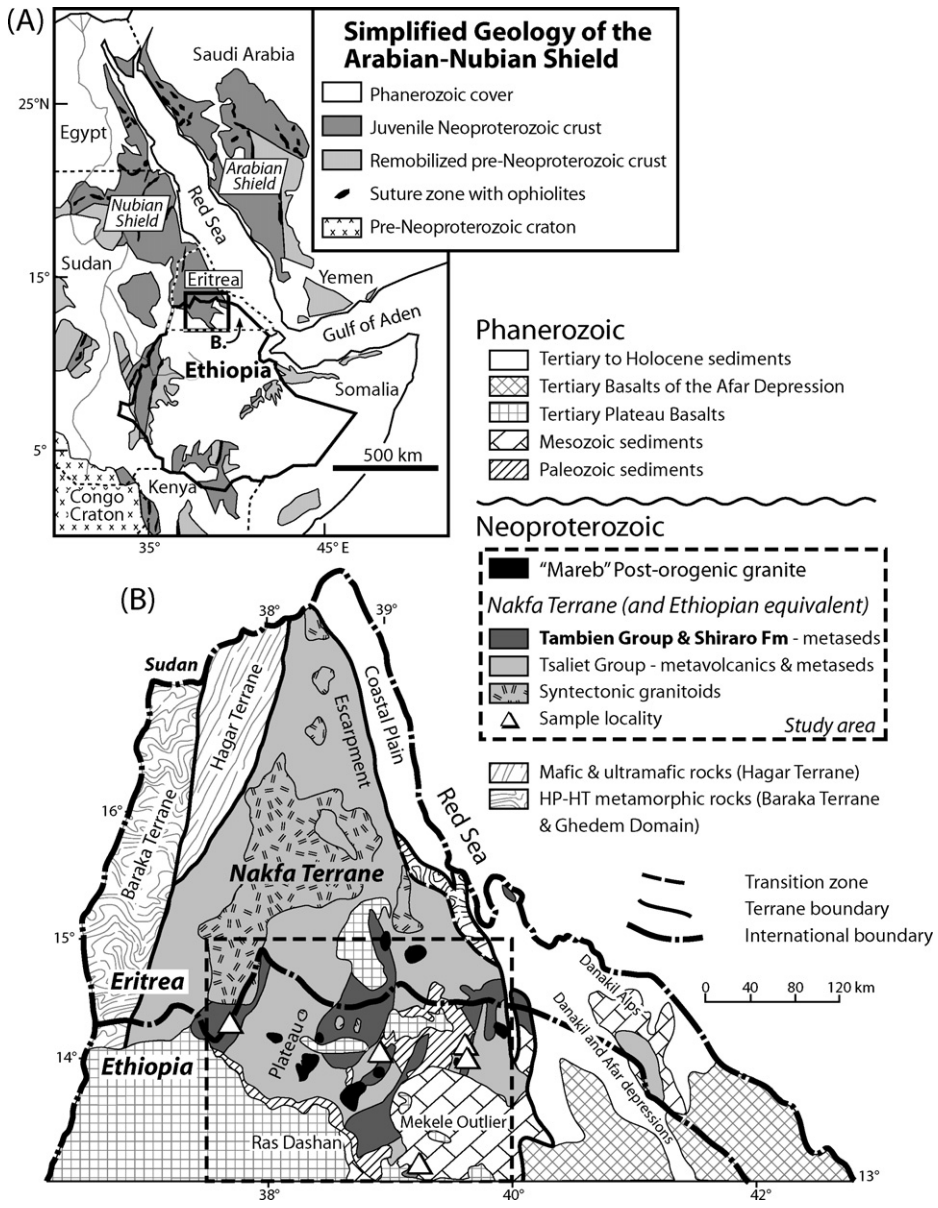

Fig. 1. (A) Northern Ethiopia study area within juvenile Neoproterozoic crust of the southern Arabian–Nubian Shield. (B) Enlargement of study area (Fig. 1A inset map) showing general geology and distribution of Tambien Group metasedimentary exposures, and study localities, within the southern extension of the Nakfa terrane.

(Beyth, 1972), whereas waning or inactive magmatism accompanied marine siliciclastic and carbonate sedimentation of the Tambien Group (Avigad et al., 2007). A second phase of post-Tambien Group magmatism generated a later suite of post-tectonic intrusives, conventionally termed 'Mareb' granitoids, which punctuated the deformed Tsaliet-Tambien system (Figs. 1B and 2; Beyth, 1972). 'Mareb' magmatism in the region likely began by ~630 Ma and continued until at least 545 Ma (Tadesse et al., 1999; Teklay et al., 2001; Asrat, 2004; Avigad et al., 2007). The post-Tambien stratigraphic record leading up to 'Mareb' intrusives is unknown due to erosion of the Neoproterozoic complex prior to deposition of Ordovician Enticho Sandstone. That 'Mareb' intrusives are post-orogenic whereas the earlier Neoproterozoic complex is deformed into NNE-trending folds and faults indicates that this time gap involved considerable collisional deformation. As the deformed Neoproterozoic complex is limited to low grade greenschist metamorphism, the EAO may have involved considerable erosion. From typical fold wavelengths, we estimate crustal shortening on the order of 200% or more. Uplift of the composite deformed and intruded Neoproterozoic complex is also indicated to account for downcutting of a vast peneplain that separates Neoproterozoic metavolcanics and metasediments from early Paleozoic mature sandstones in N. Ethiopia (Fig. 1B) and elsewhere in N. Africa and Arabia (Fig. 1 of Avigad et al., 2005).

2.2. Tectonostratigraphic setting

Fault translations of uncertain extent accompanied closure of the Mozambique Ocean and the ensuing Gondwanan collisional orogeny, as indicated by contrasting tectonostratigraphic basement terranes of the southern ANS (Fig. 1B; Vail, 1983; Drury and Berhe, 1993; Tadesse, 1997; De Souza Filho and Drury, 1998; Tsige and Abdelsalam, 2005). Tigre lies entirely within the southern extension of the Nakfa Terrane of Eritrea. The Nakfa terrane is characterized by calc-alkaline volcanics and volcaniclastic sediments, which overlie a deformed and possibly coeval plutonic complex (Drury and Berhe, 1993). In the Axum area, six petrogenetically distinct metavolcano-sedimentary blocks are delineated within the Tsaliet

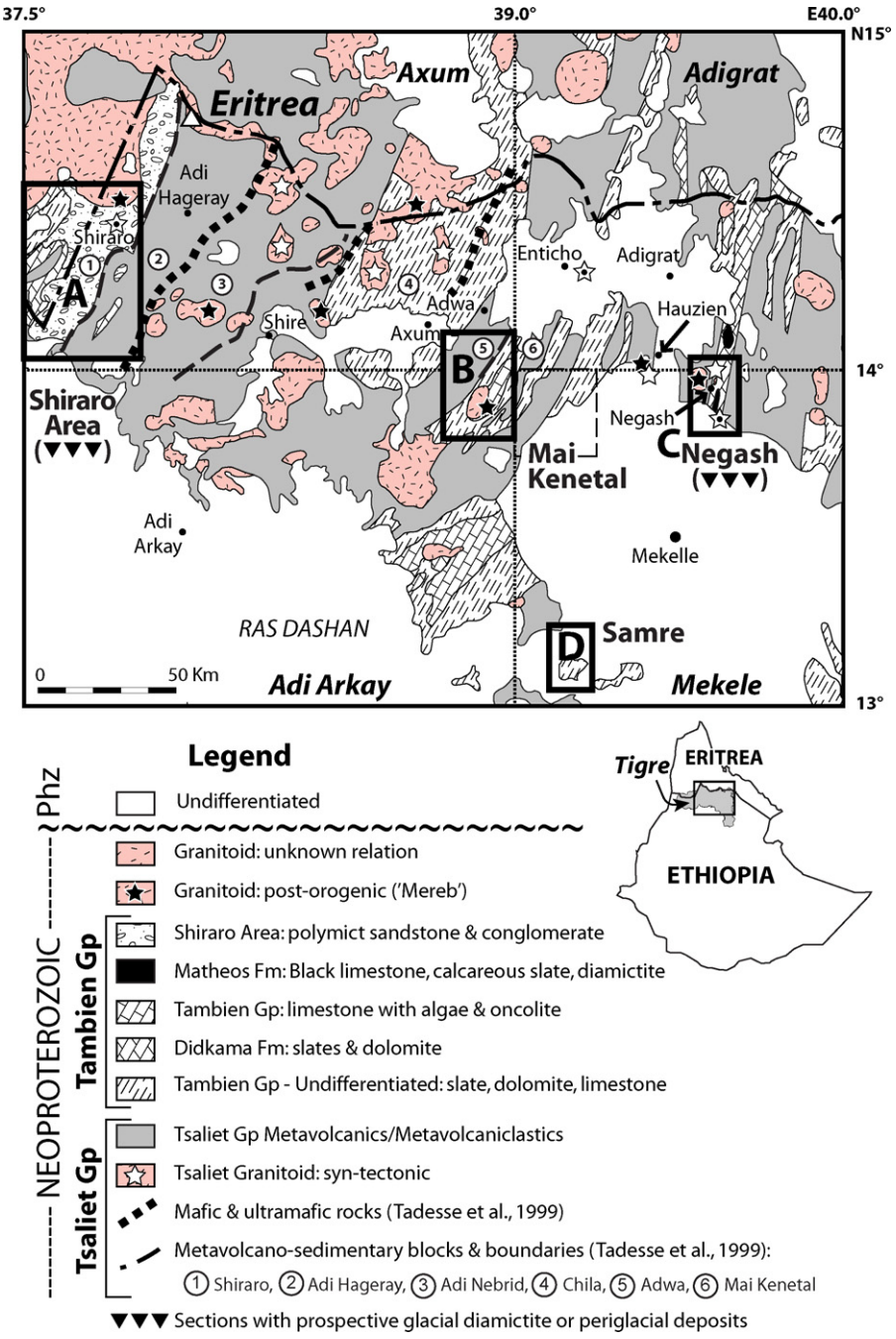

Fig. 2. General geological map of northern Ethiopia (Tigre province) showing the location of study transects (A–D) relative to Neoproterozoic supercrustal exposures (Tsaliet and Tambien Groups) and suggested microterrane associations (Tadesse et al., 1999). The prominent NE-SW structural grain developed after Tambien Group deposition in response to pan-African collisional deformation associated with development of the East African orogen. White and black stars respectively show locations of dated arc-related (syn-tectonic) and post-orogenic intrusives (Tadesse et al., 2000; Miller et al., 2003; Asrat et al., 2004), and U–Pb zircon geochronology localities sampled in association with the present study (Avigad et al., 2007, Fig. 2). The Neoproterozoic geologic framework of Tigre is known in greater detail from four 1:250,000 maps produced by the Geological Survey of Ethiopia/Ministry of Mines; *Mekele* (Arkin et al., 1971); *Adi Arkay* (Hailu, ~1972 unpublished); *Adigrat* (Garland, 1980); and *Axum* (Tadesse, 1999). These maps subdivide the greater study area into quadrants (hatched orthogonal lines). With the exception of the Axum sheet, maps were compiled prior to knowledge of Tigre's greater tectonostratigraphic context within the ANS. Lithostratigraphic subdivisions proposed for the Tambien Group vary significantly among these compilations. The Tambien Group lithologies shown are generalized from Kazmin (1972). Dashed box to the right of the Mai Kenetal study area (B), shows the Werri area studied by Sifeta et al. (2005) for chemical weathering indices.

Group (Fig. 2, circled numbers), with boundaries defined by ultramafic belts and major structural changes (Tadesse et al., 1999). These were interpreted as originating as a succession of westward-accreted intra-oceanic arcs. We recognize that the name 'Tsaliet Group' combines these Nakfa sub-terranes, but use this name for the sake of convenience. The predominantly marine lithofacies associated with the Tambien Group indicate that it was deposited on a magmatically inactive arc-accretion complex following terrane accretion (Avigad et al., 2007).

2.3. Tambien Group lithostratigraphy

Lithostratigraphic organization and regional correlation of the Tambien Group throughout Tigre are unresolved. The thin-bedded,

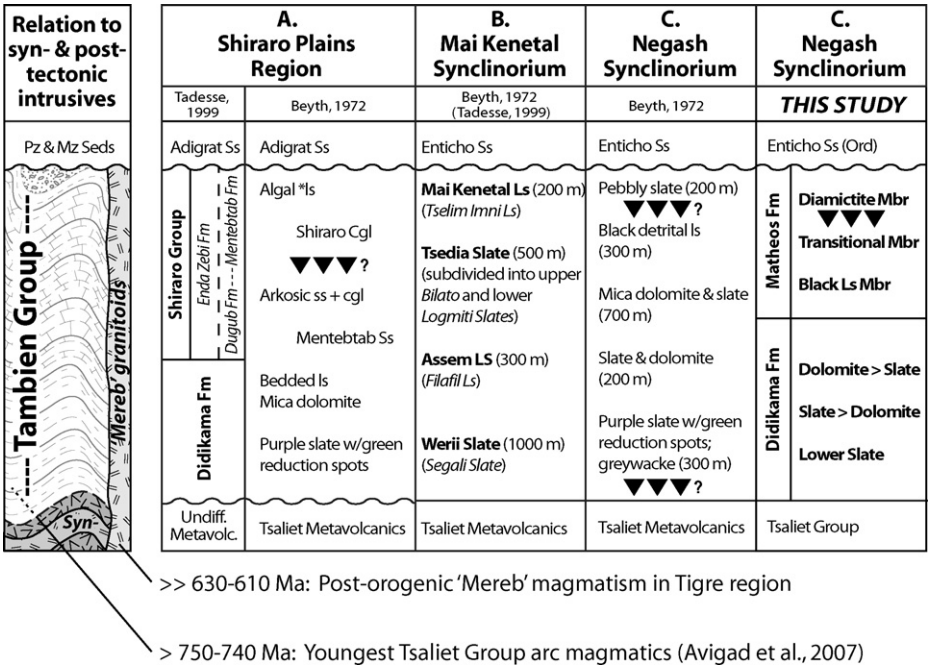

Fig. 3. Regional stratigraphic subdivision of the Tambien Group and relation to syn- and post-tectonic intrusives. Beyth (1972) originally suggested that glacial diamictites occur within the Tambien Group at Shiraro and Negash localities (A and C). The upper Algal Limestone unit in the Shiraro Plains Region was originally termed the "Algal, stromatoporoidea (?) limestone" in Beyth (1972). Stromatoporoids (Cambrian to Cretaceous) can now be excluded for this unit. The Tambien Group was deposited after Tsaliet Group arc magmatism waned (775–740 Ma) and prior to post-orogenic 'Mareb' magmatism (»630 Ma); age relations from Avigad et al. (2007).

fine-grained, and lithologically heterogenous nature of many Tambien units, all subject to various low-grade diagenetic modifications and without biostratigraphically useful (macroscopic) fossils, makes them difficult to correlate. Very few way-up indicators are evident and it is mainly fining upward sequences and phototropic organosedimentary structures (columnar/domal stromatolites) in carbonate units that preserve the up-direction of sedimentation. The tightly folded (often overturned) and faulted character of Neoproterozoic basement throughout Tigre, and lack of radiometric ages, further add to the challenge of deciphering internal stratigraphy. Tambien Group exposures are best studied in Mai Kenetal and Negash synclinoria (Fig. 2; Arkin et al., 1971; Beyth, 1972; Tadesse, 1999; Alene et al., 1999; Miller et al., 2003; Beyth et al., 2003), where basal Tambien Group sediments are well exposed. Both of these Tambien sequences show an overall upsection increase in the abundance of carbonate, and are intruded by 'Mareb' granites that provide minimum age constraints. Tuffaceous beds or metabentonites are not detected in either sequence above their transitional base with the Tsaliet Group, consistent with Tambien carbonate deposition marking a lull in igneous activity (Avigad et al., 2007).

Tambien Group outcrops occur in lowlands of the western Shiraro area, in several *en echelon* synclinoria to the east (*i.e.*, Mai Kenetal, Tsedia, Chemit, and Negash), and the Red Sea Escarpment area east of Adigrat (Beyth, 1972; Fig. 2). Apparent regional facies variations occur within the internal stratigraphy of the Tambien Group, and Beyth (1972) proposed a preliminary correlation for three areas: Shiraro in the west (study area A), Mai Kenetal synclinorium in the center (study area B), and Negash synclinorium in the east (study area C; Figs. 2 and 3). Polymictic conglomerates and pebbly slates of possible peri-glacial and glacial origin occur high in the Shiraro and Negash sequences. The lower slate-dominated portion of the Tambien Group also bears polymictic agglomerates and greywacke of possible glacial association (Beyth, 1972; Beyth et al., 2003). Four formations were identified within the Tambien Group based on the Mai Kenetal type section (western flank near 13°55′N, 38°50′E). From base-to-top these include the Werii Slate, Assem Limestone, Tsedia Slate, and Mai Kenetal Limestone. In Negash synclinorium, the Tambien sequence includes slate and interbedded dolomite-slate below black limestone, which in turn grades upward into non-calcareous slate and eventually pebbly slate (diamictite). The Mai Kenetal section may correlate with these "Negash facies" (Beyth, 1972), and similar dolomite-slate successions were subsequently documented in the escarpment east of Adigrat, as well as in synclines in the Shiraro area.

Fig. 3 shows Beyth's (1972) original lithostratigraphic framework for the Tambien Group in the Shiraro Area, and Mai Kenetal and Negash synclinoria, and subsequent terminologies proposed during compilations of the Adi Arkay, Adigrat, and Axum sheet maps (map boundaries shown in Fig. 4). During compilation of the Adigrat map, the Tsaliet Metavolcanics were formalized as the Tsaliet Group, and the Tambien Group in Negash synclinorium was subdivided into the lower Didikama Formation (after similar dolomitic rocks in the Shiraro Area) and overlying Matheos Formation (equivalent to Beyth's informal black detrital limestone, and pebbly slate/diamictite facies; Garland, 1980). This subdivision for Negash, integrated with Beyth's informal facies terminology, was used in subsequent publications (Miller et al., 2003; Beyth et al., 2003; Alene et al., 2006; Avigad et al., 2007). We employ a similar framework (Fig. 3), but suggest that the Matheos Formation can be differentiated into three members: Black Limestone, Transition, and Diamictite (Fig. 3). In subsequent mapping of Mai Kenetal synclinorium for the Axum map, Tadesse (1999) used local names to address the possibility that some of Beyth's type areas extended to Mai Kenetal units (*i.e.*, Werii Slate, Tsedia Slate) might reside in different tectonostratigraphic blocks. The main difference between the two lithostratigraphic schemes is differentiation of Beyth's Tsedia Slate into lower Logmiti Slate and overlying Bilato Limestone and Slate (Fig. 3B). Tadesse (1999) also formalized a new stratigraphic scheme for the Shiraro area (Fig. 3A), splitting Beyth's informal Tambien Group facies into the basal Didikama Formation and overlying Shiraro Group. Within the latter, three metasiliclastic formations were designated (Enda Zebi, Dugub, and Mentebteb formations), each with respective lateral facies variations.

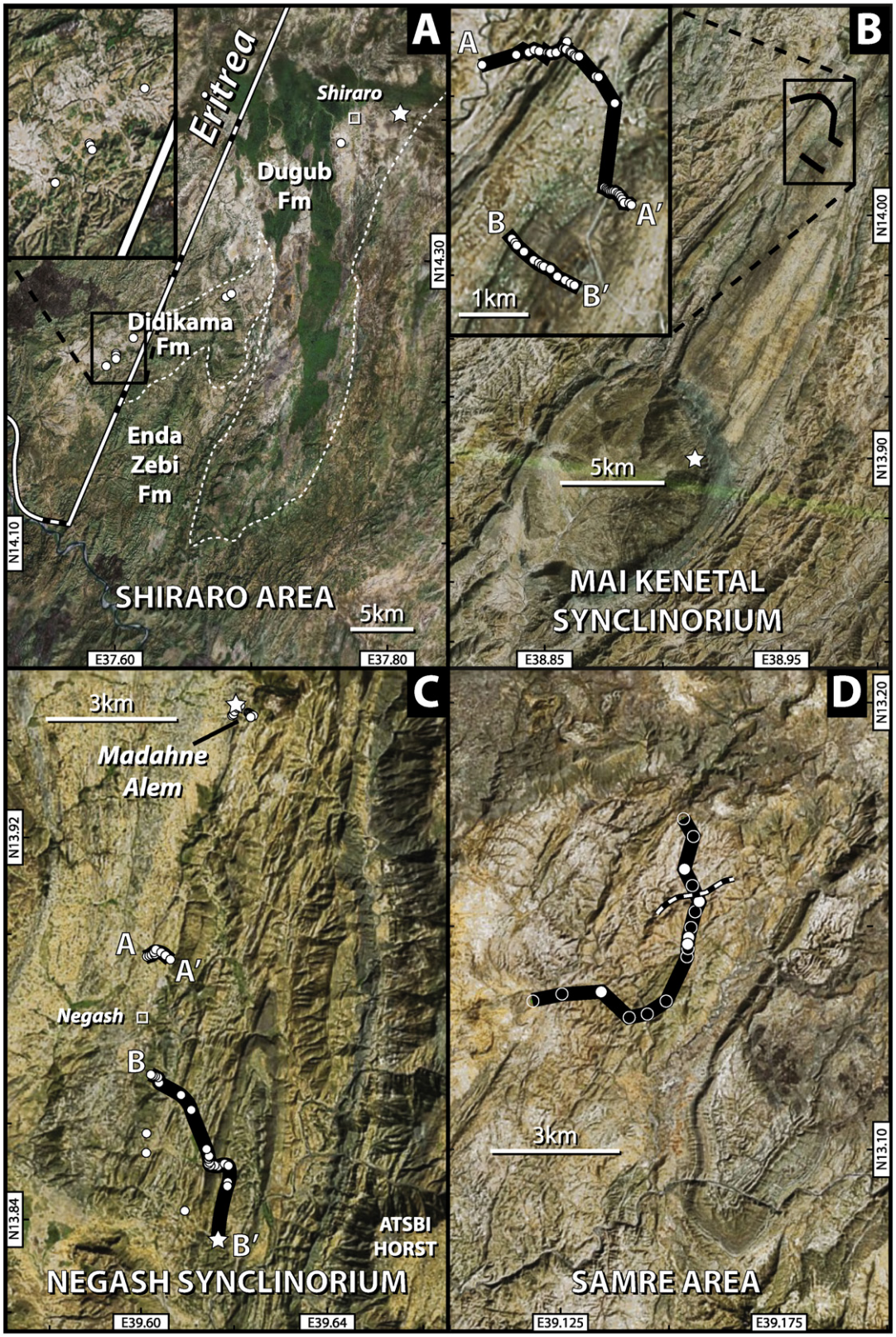

Fig. 4. Satellite images of Tambien Group study localities showing transect and geochronology sample (stars) localities. North is to the top of all images. (A) Shiraro area carbonate ridge (mapped as Didikama Formation) and diamictite (Dugub Fm = Shiraro Molasse = Shiraro Conglomerate) localities; map boundaries approximated from Axum Sheet map (Tadesse, 1999). (B) Mai Kenetal synclinorium western limb transects A–A′ and B–B′ and granitoid U–Pb zircon sample. (C) Negash synclinorium western limb transects A–A′, B–B′ and Madahne Alem. Samples collected immediately west of transect B–B′ (Miller et al., 2003) and in the eastern limb (EL) have negative $\delta^{13}C_{carb}$ compositions. Madahne Alem locality contains a concordant felsic metasandstone unit (star) sampled for zircon U–Pb geochronology. (D) Samre area reconnaissance transect through the upper Tsaliet Group and lower Didikama Formation, within the western limb of a possible synclinorium. The dashed line approximates the contact between the Tsaliet and Tambien Groups. Solid white dots indicated sampled localities.

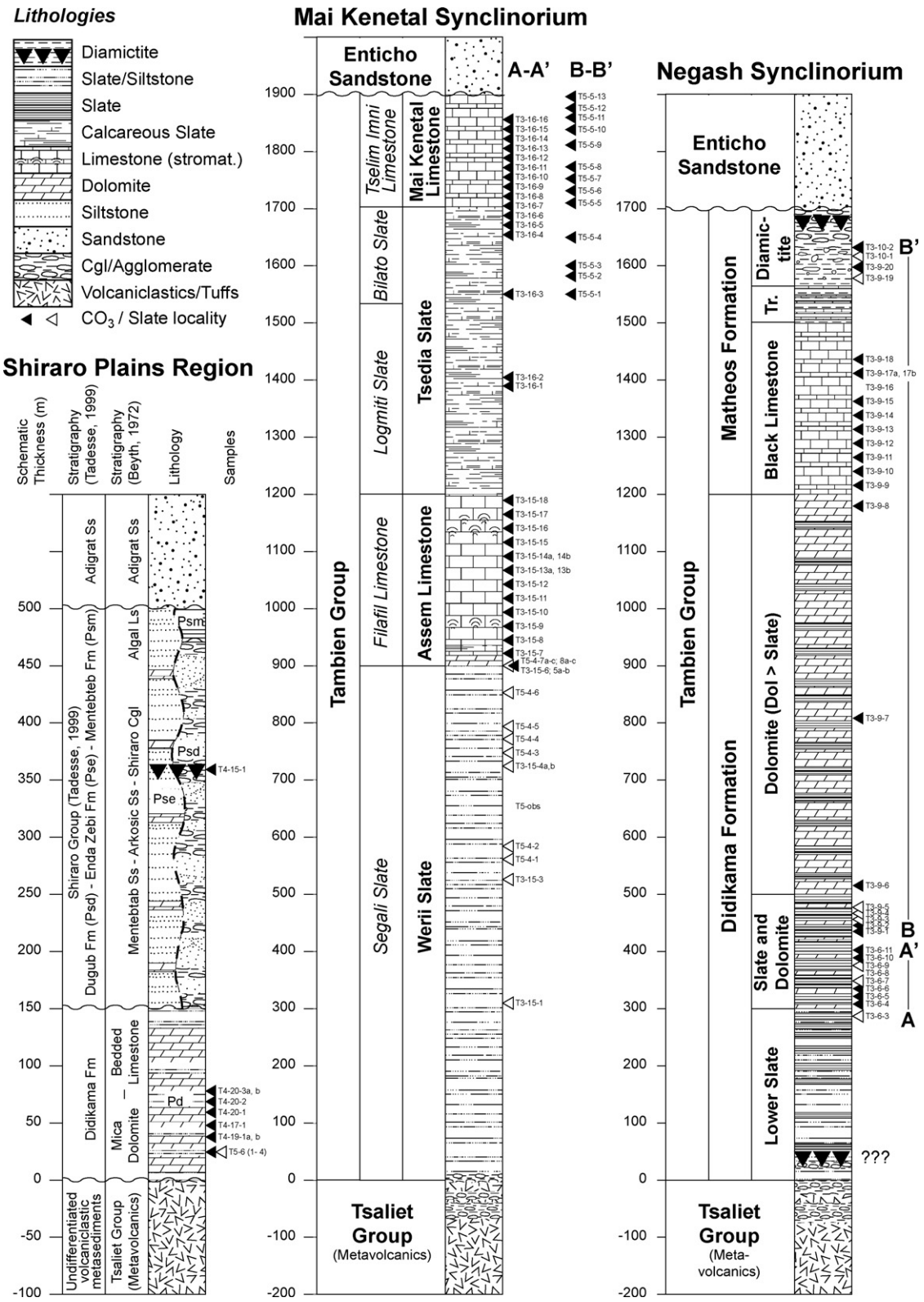

Fig. 5. Generalized composite stratigraphic sections for Tambien Group transects showing sample datums within lithostratigraphic units. Shiraro area stratigraphic thicknesses are taken from Tadesse (1999; Axum sheet map) with sample elevations estimated from field relations. Mai Kenetal and Negash stratigraphic columns follow Beyth (1972), with sample positions interpolated within Tambien units from GPS-field relations and satellite imagery. Madahne Alem and Samre transect columns compiled from GPS-field relations and satellite imagery. Triangles adjacent to sample codes denote carbonate (black) and slate (white—for PIA weathering indices) lithologies. Note the expanded vertical scale for Shiraro and Madahne Alem localities.

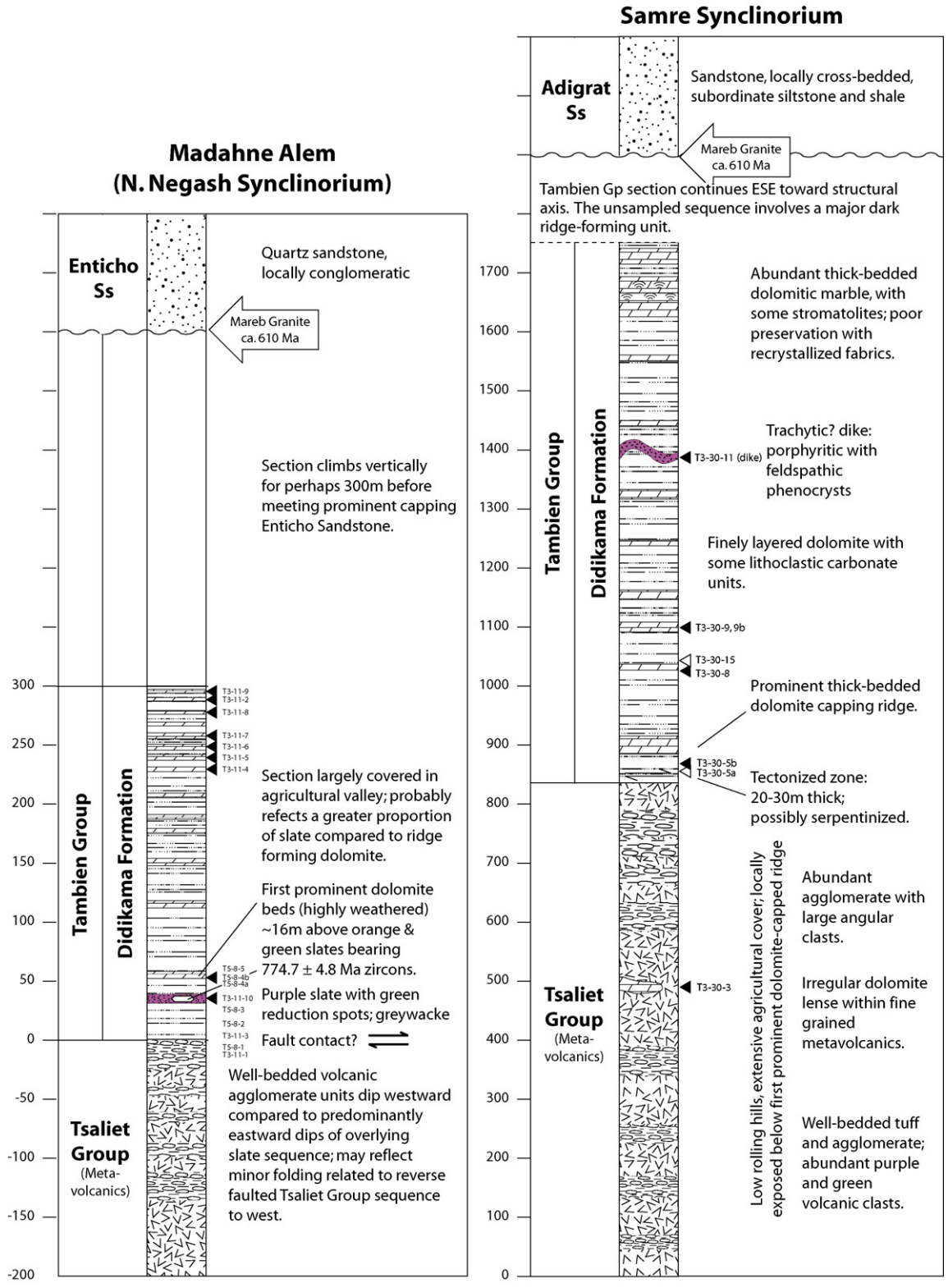

Fig. 5. (*Continued*).

2.4. Tambien Group age and Cryogenian glacigenic associations

Depositional age of the Tambien Group is constrained primarily from radiometric dating of the underlying Tsaliet Group (metavolcanics and syn-tectonic granitoids) and post-orogenic 'Mareb' granitoids. The range of available dates, including new dates in Avigad et al., 2007, indicates that Tambien Group carbonate deposition in N. Ethiopia began as Tsaliet arc magmatism waned (*c.* 775–740 Ma) and before intrusion of 'Mareb' plutons. The onset of 'Mareb' magmatism is poorly dated regionally but available ages are *c.* 610 ± 10 Ma in eastern Tigre (Miller et al., 2003; Asrat, 2004) and *c.* 630 ± 10 Ma in Eritrea (Teklay et al., 2001). These age con-

straints allow the Tambien Group to include all but the youngest (580 Ma Gaskiers) Neoproterozoic glaciation. The minimum age for Tambien Group exposures (*i.e.*, Matheos Formation diamictite, Negash synclinorium) is likely significantly older than 'Mareb' magmatism (*i.e.*, 630–610 Ma) within Tigre, considering that the time gap between youngest preserved Tambien deposits and 'Mareb' intrusions must have involved significant orogenesis and crustal thickening.

Tambien Group metasediments collected in a reconnaissance survey of the Negash synclinorium were inferred to correspond to "Sturtian" age Snowball Earth events (Miller et al., 2003). Here, a pronounced negative carbon isotope excursion from values of +7 to at least −2‰ accompanies the transition from marine carbonate to diamictite deposition. An affiliated "cap" carbonate is not identified in the Negash structure. Matheos Formation black limestone underlying the diamictite had an average $^{87}Sr/^{86}Sr$ of 0.7066, consistent with "Sturtian" (*c.* 750–720 Ma) ages on the reference curve of Jacobsen and Kaufman (1999). Age models for this reference curve have been subsequently reinterpreted, and there are important new radiometric ages constraining the timing of Cryogenian glaciations, particularly those conventionally binned as "Sturtian" (*e.g.*, Kendall et al., 2006; Fanning, 2006; Halverson, 2006; Hoffmann et al., 2006) or pre-Marinoan. The latter range between ~755 and 640 Ma, arguing against a single discrete episode of pre-Marinoan glaciation. In recognition of this ambiguity, we consistently use the term "Sturtian" in quotes. The closest well constrained "Sturtian" glacial deposits belong to the Ghubrah Formation (Abu Mahara Group) in Oman, which contains ~713 Ma volcaniclastic rocks (Bowring et al., 2007). Preliminary studies of Mai Kenetal and synclinoria to the east (Tsedia) also support a pre-"Sturtian" timeframe for the Tambien Group, and indicate a lower interval with negative $\delta^{13}C$ (Miller et al., 2003, 2004a,b; Alene et al., 2006). However, the specific "Sturtian" glacigenic affinity and depositional age of the Tambien Group remain relatively unconstrained (see also Avigad et al., 2007).

3. Objectives and new Tambien Group localities

To improve regional correlations and better understand the Tambien Group in relation to Cryogenian tectonic, climatic, and biological episodes, we compiled litho- and chemostratigraphic profiles for Beyth's original focus areas, in addition to a new southern locality (Samre; Fig. 2). For each location we establish essential stratigraphy, sedimentology, and chemistry ($\delta^{13}C$, $^{87}Sr/^{86}Sr$, $\delta^{18}O$, [Fe], [Mn], [Sr]) to aid correlation with other successions, and critically assess sample preservation. We focus on Mai Kenetal and Negash synclinoria as these structures were mapped in some detail (Beyth, 1972; Tadesse, 1999; Beyth et al., 2003). These localities share similar lithostratigraphies above Tsaliet Group metavolcanics, including distinct black carbonate units high in the sequence, but their correlations are unresolved. The lower portion of the Mai Kenetal type section is of particular importance because, unlike Negash, most of its carbonate lithofacies are limestone. Fig. 4 shows satellite images of the four investigated areas (A–D, cf. Fig. 2) and the locations of stratigraphic transects. Fig. 5 shows corresponding stratigraphic columns following Beyth (1972) with sampled datums approximated from georeferenced satellite imagery and GPS sample coordinates. Schematic cross-sections showing lithostratigraphic sample positions are also shown for each locality (except Samre) in supplemental online material, further described in Section 6 (*Results*). Note that text references to supplementary figures have an "S" prefix. We estimate that depocenters within the composite study area were likely distributed across a NW-SE distance no less than 425 km prior to collisional deformation (based on 200% shortening).

3.1. Shiraro area (Area A)

The Shiraro area, close to the border with Eritrea (130 km WNW of Mai Kenetal), is a graben containing Tigre's westernmost exposures of Neoproterozoic metasediments (Fig. 4A, S8), including prospective peri-glacial units, stratigraphically bracketed by carbonates (Fig. 3A). Weakly metamorphosed and locally folded siliciclastic units of the Shiraro Group are widespread throughout western Tigre but we did not find contacts with bounding carbonates. We investigated two intervals of the Tambien Group lithostratigraphic sequence. To the south, near the Eritrean border and parallel to the main Humera-Shiraro road, we sampled low NE-trending carbonate ridges mapped as Didikama Formation (Tadesse, 1999; Fig. 4A inset). Our principal localities (T4-19, T4-20, T5-6) are within 3 km, along strike, and we estimate that they collectively derive from the lower 80 m of the exposed carbonate outcrop belt. The sampled ridges consist of sub-meter thick resistant carbonate beds (Fig. S8E) with thinner recessive intercalated slates. Underlying the sampled ridges, in the road plain, are mainly non-calcareous slates. The composite outcrop belt, a mixed carbonate-siliciclastic sequence, is thus broadly consistent with the Didikama Formation. Comparable localities further NE (T4-17, T4-18) were structurally disturbed dolomitic breccias and were excluded from further study. East of Shiraro we examined arkosic sandstone and polymictic conglomerates of the younger Dugub Fm (Shiraro Group, star symbol in Fig. 4A), with detrital U–Pb zircon ages for this unit published in Avigad et al. (2007). A stratigraphically higher limestone unit was not seen in the area (the algal limestone facies of Beyth, 1972; see Fig. 3A).

3.2. Mai Kenetal synclinorium (Area B)

Mai Kenetal is a 10 × 40 km, SW-trending, doubly plunging synclinorium (Fig. 4B), the center of which is penetrated by a large (7–9 km diameter) post-orogenic 612 Ma 'Mareb' granitoid (Avigad et al., 2007). The Tambien Group is well exposed NE of the intrusion. We sampled the NW limb in two subparallel transects (A–A′ and B–B′, Fig. 4B inset, S9) near the NE extent of the structure, where SE-dipping exposures of the Tambien Group are nearly continuous. Transect A–A′ began in Werii Slate at Seysa River and culminated in Mai Kenetal Limestone near the local synclinorial axis. Transect B–B′ offered better access to the upper Tsedia Slate (Bilato Limestone and Slate) and youngest remnants of the Mai Kenetal Limestone.

3.3. Negash synclinorium (Area C)

Negash is an elongate (5 km wide × 30 km long) SSW-plunging, west dipping, slightly overturned synclinorium (Fig. 4C). It is bounded to the east by normal faults of the Atsbi Horst. The western synclinorial boundary is defined by a reverse fault that marks the Tsaliet-Tambien contact (Beyth et al., 2003). Reverse faulting may also occur within the basal Tambien sequence. The core of the syncline exposes diamictite (uppermost Matheos Formation) at its southern extent near Adi Geyno River. We sampled the Tambien sequence in two western limb locations; at Madahne Alem (Fig. S11), where the Tambien transition from slates to basal carbonates is well exposed, and in a more southerly compound transect (Negash A–A′, B–B′; Fig. S12) through the higher Tambien sequence. At Madahne Alem (13.9456N, 39.6182E) we sampled basal Tambien slates and dolomites (lowest Didikama Formation) above a distinctive interval of polymict volcanic agglomerates and slates. Negash A–A′ began (along strike 5.6 km SSW of Madahne Alem) in the Didikama Formation and culminated at a small (0.75 × 2 km) 'Mareb' granitoid. Negash B–B′ resumed along strike 2.6 km further SSW, beginning in lower Didikama dolomites and slates and

Table 1
Chemostratigraphic data for Tambien Group localities.

Transect/sample ID	Unit	Height[a] (m)	Sample description[b] (microdrilled mineralogy)	Alt[c]	$^{87}Sr/^{86}Sr$	[d]N	CO_3[e] min	Mg/Ca (mol)	Sol[f] (wt%)	Ca (wt%)	Mg (wt%)	Sr (ppm)	Fe (ppm)	Mn (ppm)	$\delta^{13}C_{carb}$[g] (‰)	$\delta^{18}O_{carb}$[g] (‰)	$\delta^{13}C_{org}$[g] (‰)	ε_{TOC}[h] (‰)	TOC[i] (wt%)	PIA[j]
Shiraro area																				
T4-15-01	Shiraro Cgl	360.0	Arkosic sandstone; youngest concordant grain is 739 ± 6 Ma (Avigad et al., 2006)																	
T4-20-03a	Didikama Fm	78.0	Pelloidal PS (brown altered NFC)	*	0.706718 ± 18	2	C	0.01	86	37.38	0.14	125	944	1704	−0.96	−13.15	−27.34	27.12	0.01	
	Didikama Fm	78.0	Pelloidal PS (FC)		0.706129 ± 20	2	C	0.09	90	36.52	2.04	682	16,602	4732	−2.78	−5.87				
T4-20-03b																				
T4-20-02	Didikama Fm	69.0	Intraclastic PS (FC)		0.706134 ± 23	3	C	0.03	92	38.33	0.71	529	4,568	2212	−3.29	−12.39	−27.98	25.40	0.02	
T4-20-01	Didikama Fm	60.0	Pelloidal PS	*	0.705667 ± 21	3	C	0.06	92	36.92	1.33	360	4,500	2223	1.60	−10.13	−27.07	29.47	0.01	
T4-19-01a	Didikama Fm	38.0	Intraclastic GS (NFC)	*	0.706292 ± 21	2	C	0.01	89	37.71	0.17	129	2,233	1943	−0.38	−11.03	−22.75	22.89	0.02	
T4-19-01b	Didikama Fm	38.0	Intraclastic GS (FC)		0.706063 ± 16	3	C	0.05	94	35.18	1.11	373	9,094	2124	−3.07	−6.96				
T5-06-04	Didikama Fm	27.0	Slate																	
T5-06-03	Didikama Fm	26.0	Intraclastic MS w/compound micropeloidal grains		0.706090 ± 10	1	D>C	0.65	96	28.10	11.12	473	20,759	3350	3.80	−11.32	−25.51	30.08	0.04	
T5-06-02	Didikama Fm	24.0	Micropeloidal PS/GS (FC)		0.706096 ± 10	1	C	0.10	91	37.56	2.27	643	18,342	4404	3.95	−11.82	−21.25	25.75	0.05	
T5-06-01a	Didikama Fm	20.3	Intraclastic micropeloidal PS/GS (FC)		0.706160 ± 08	1	C	0.03	88	39.59	0.66	703	11,378	4369	2.99	−12.41	−22.50	26.08	0.04	
	Didikama Fm	20.0	Slate																	
T5-06-01b																				
Mai Kenetal B–B′																				
T5-5-13	Mai Kenetal LS	1896.0	Relict texture of micropeloidal PS/GS? (FC)		0.706726 ± 09	1	C	0.02	100	41.42	0.48	2743	86	20	6.64	−3.67	−28.39	36.05	0.13	
T5-5-12	Mai Kenetal LS	1875.0	Pelloidal PS/microbial BS? (NFC)		0.706724 ± 09	1	C	0.01	100	41.02	0.31	1961	573	53	4.44	−3.64	−24.43	29.59	0.09	
T5-5-11	Mai Kenetal LS	1859.0	Micropeloidal MS		0.706723 ± 10	1	C	0.03	95	41.40	0.87	1840	1,405	86	4.83	−4.38	−24.92	30.51	0.10	
T5-5-10	Mai Kenetal LS	1,838.0	Laminated MS		0.706704 ± 08	1	C	0.09	89	40.08	2.24	1900	3,528	172	5.06	−6.83	−24.99	30.82	0.31	
T5-5-9	Mai Kenetal LS	1810.0	Micropeloidal PS?		0.706735 ± 07	1	C	0.01	97	41.22	0.18	2781	1,307	106	5.46	−7.63	−21.92	27.99	0.16	
T5-5-8	Mai Kenetal LS	1773.0	MS, DL		0.706726 ± 08	1	C	0.01	89	43.35	0.29	2722	2,187	332	5.56	−9.30	−24.35	30.66	0.23	
T5-5-7	Mai Kenetal LS	1752.0	MS		0.706732 ± 09	1	C	0.02	93	38.99	0.40	2903	2,017	191	5.32	−9.77	−24.13	30.18	0.15	
T5-5-6	Mai Kenetal LS	1731.0	Laminated MS/microbial BS?		0.706735 ± 08	1	C	0.03	99	40.25	0.61	2839	1,477	152	5.65	−7.33	−24.26	30.65	0.14	
T5-5-5	Mai Kenetal LS	1,710.0	Laminated MS		0.706725 ± 09	1	C	0.04	96	39.44	0.95	2018	2,492	159	5.49	−8.53	−23.34	29.52	0.14	
T5-5-4	Mai Kenetal LS	1,649.0	MS		0.706710 ± 08	1	C	0.01	88	40.81	0.33	2397	1,654	436	5.28	−8.78	−24.54	30.57	0.24	
T5-5-3	Mai Kenetal LS	1600.0	MS		0.706674 ± 06	1	C	0.14	88	36.84	3.23	2769	8,123	279	5.00	−7.16	−24.97	30.74	0.20	
T5-5-2	Mai Kenetal LS	1582.0	MS		0.706647 ± 09	1	C	0.02	92	39.45	0.46	2178	2,763	321	7.22	−9.18	−24.51	32.53	0.12	
T5-5-1	Tsedia Slate	1550.0	MS (FC + Dol? in matrix/fractures)	*	0.705813 ± 09	1	C	0.14	88	35.01	2.92	1516	14,609	1133	7.27	−9.00	−25.91	34.06	0.17	
Mai Kenetal A–A′																				
T3-17-01	"Mareb" Granitoid	na	Granite–Zircon U–Pb age of 612.3 ± 5.7 Ma (Avigad et al., 2006)																	
T3-16-16	Mai Kenetal LS	1855.0	Micropeloidal WS, DL, organic rich		0.706746 ± 15	2	C	0.01	95	34.71	0.20	2323	1,100	85	4.77	−3.26	−28.35	34.09	0.10	
T3-16-15	Mai Kenetal LS	1839.0	Micropeloidal MS/WS, IL, organic rich		0.706721 ± 16	2	C	0.01	95	40.36	0.18	1891	1,933	62	5.52	−5.85	−25.99	32.35	0.15	
T3-16-13	Mai Kenetal LS	1805.0	Laminated MS/micropeloidal WS, organic rich		0.706789 ± 14	2	C	0.02	86	39.32	0.56	2577	3,353	232	6.27	−9.97	−25.92	33.04	0.11	

T3-16-12	Mai Kenetal LS	1788.0	Intraclastic GS/PS, organic rich		0.706780 ± 15	2	C	0.04	99	35.95	0.85	2465	1,969	163	4.54	−6.58	−23.90	29.13	0.14	
T3-16-11	Mai Kenetal LS	1772.0	Intraclastic WS/PS, organic rich		0.706711 ± 15	2	C	0.01	92	39.72	0.26	2896	2,229	405	4.96	−9.97	−26.66	32.49	0.10	
T3-16-10	Mai Kenetal LS	1755.0	Micropeloidal WS, organic rich		0.706730 ± 16	3	C	0.02	90	39.30	0.38	2309	2,871	152	4.96	−8.85	−24.40	30.09	0.14	
T3-16-09	Mai Kenetal LS	1739.0	Intraclastic GS, organic rich		0.706736 ± 15	2	C	0.04	99	38.32	1.00	2101	1,935	179			−24.66		0.18	
T3-16-08	Mai Kenetal LS	1721.0	MS/micropeloidal WS		0.706749 ± 27	3	C	0.02	68	41.16	0.60	3019	7,763	564	4.82	−6.68	−29.17	35.01	0.09	
T3-16-07	Mai Kenetal LS	1705.0	Intraclastic GS, organic rich		0.706766 ± 18	3	C	0.01	98	40.72	0.32	2072	1,072	135	4.49	−5.25	−25.48	30.75	0.19	
T3-16-06	Mai Kenetal LS	1689.0	Intraclastic GS, organic rich		0.706808 ± 24	2	C	0.01	94	39.79	0.36	2737	1,348	181	5.70	−8.93	−24.52	30.98	0.22	
T3-16-05	Mai Kenetal LS	1671.0	MS/WS		0.706774 ± 19	2	C	0.02	94	39.79	0.36	2597	1,923	138	5.56	−9.00	−26.60	33.04	0.10	
T3-16-04	Mai Kenetal LS	1654.0	Intraclastic WS		0.706744 ± 15	2	C	0.03	85	39.79	0.36	2018	2,413	207	5.29	−10.22	−25.18	31.26	0.06	
T3-16-03	Tsedia Slate	1550.0	MS, organic rich	*?	0.706151 ± 16	2	C > D	0.41	48	27.68	6.89	1759	34,774	2860	2.27	−7.99	−24.96	27.93	0.28	
T3-16-02	Tsedia Slate	1405.0	Intraclastic MS?		0.706330 ± 23	2	C	0.02	82	41.49	0.40	1133	4,121	618	1.90	−10.82	−27.14	29.85	0.06	
T3-16-01	Tsedia Slate	1390.0	Calcareous slate, laminated		0.706312 ± 14	2	C	0.03	45	37.61	0.67	1262	13,984	2496	1.13	−13.06	−24.68	26.47	0.04	
T3-15-18	Assem LS	1189.0	Microbial BS/stromatolite	*	0.705946 ± 13	2	C	0.06	96	41.36	1.42	299	2,206	500	−1.22	−12.67	−29.05	28.66	0.01	
T3-15-17	Assem LS	1165.0	Microbial BS/stromatolite		0.706132 ± 16	2	C > D	0.20	97	35.34	4.18	192	902	131	−0.72	-11.67	-28.44	28.54	0.01	
T3-15-16	Assem LS	1140.0	Dolospar/microspar, replaced fabric	*	0.705900 ± 14	2	D	0.91	95	22.47	12.39	87	1,129	123	−2.08	−5.30	−40.32	39.85	0.02	
T3-15-15	Assem LS	1116.0	Micropeloidal MS/WS/microbial BS?, dolomitic		0.706165 ± 14	2	C > D	0.15	99	37.61	3.43	164	696	72	−2.17	−9.39	−26.48	24.97	0.02	
T3-15-14	Assem LS	1091.2	Microbial BS/MS		0.706173 ± 16	2	C	0.04	99	41.77	0.98	225	568	58	−1.68	−11.63				
T3-15-14b	Assem LS	1091.0	Intraclastic GS (dolomitized clast sampled)	*	0.705948 ± 12	2	D > C	0.57	89	27.95	9.65	182	4,161	165	−1.16	−10.19	−31.39	31.21	0.02	
T3-15-14b	Assem LS	1091.0	Intraclastic GS (NFC)		0.706298 ± 13	2	C	0.01	96	43.95	0.25	354	845	61	−1.92	−8.60				
T3-15-13b	Assem LS	1067.2	Layered MS, partially replaced by dolomite	*	0.706319 ± 17	2	C > D	0.30	94	31.99	5.91	198	4,850	270	−1.43	−8.84	−29.52	28.95	0.03	
T3-15-13	Assem LS	1067.0	Intraclastic GS/microbial BS?, organic rich		0.706215 ± 15	2	C	0.02	98	42.56	0.45	307	333	46	−1.74	−9.55	−27.38	26.37	0.13	
T3-15-12	Assem LS	1043.0	Cryptic fabric, micropeloidal PS or GS?		0.706151 ± 14	2	C	0.01	99	42.99	0.18	138	626	101	−4.09	−7.74	−31.00	27.77	0.02	
T3-15-11	Assem LS	1018.0	Intraclastic GS?; organic rich		0.706084 ± 13	2	C	0.01	98	42.47	0.29	452	345	47	−1.72	−11.47	−27.07	26.06	0.17	
T3-15-10	Assem LS	994.0	Micropeloidal/micro-oncoidal GS/PS		0.706050 ± 13	2	C	0.01	99	43.69	0.14	270	167	55	−1.75	−8.68	−33.68	33.04	0.04	
T3-15-09	Assem LS	969.0	MS		0.706312 ± 17	2	C	0.01	97	42.52	0.20	264	855	221	−2.17	−8.18	−37.35	36.55	0.04	
T3-15-08	Assem LS	945.0	MS		0.706422 ± 14	2	C	0.01	98	44.21	0.17	227	875	294	−1.27	−9.11	−32.36	32.13	0.02	
T3-15-07	Assem LS	907.0	Slate, calcareous	*	0.708441 ± 13	1	C > D	0.23	15	30.07	4.20	964	42,014	1647						
T5-04-07b	Assem LS	902.0	Slate, non-calcareous																	78
T5-04-08c	Assem LS	900.9	MS (dolomicrospar)	*	0.706685 ± 08	1	C > D	0.39	73	29.03	6.90	851	13,239	3463	0.48	−9.64	−27.36	28.62	0.03	
T5-04-08b	Assem LS	900.5	Micropeloidal PS/GS (Dolo GS fabric)		0.705970 ± 09	1	D>C	0.52	93	27.89	8.79	344	6,389	2357	0.32	−7.35	−27.74	28.86	0.08	
T5-04-08a	Assem LS	900.1	Micropeloidal PS/GS (Dolo GS fabric + late FC)		0.705978 ± 09	1	C > D	0.41	94	30.76	7.61	340	5,427	2386	−0.50	−7.90	−26.70	26.92	0.13	
T3-15-05a	Assem LS	900.0	Micropeloidal GS (Dol)		0.706322 ± 13	2	D > C	0.61	99	26.20	9.72	315	4,364	1604	−2.24	−6.13	−31.24	29.94	0.05	
T3-15-05b	Assem LS	900.0	Calcareous slate, laminated	*	0.707129 ± 15	1	C	0.15	29	34.30	3.03	1337	23,107	3815	−3.84	−11.83	−26.17	22.93	0.04	

Table 1 (*Continued*)

Transect/sample ID	Unit	Height[a] (m)	Sample description[b] (microdrilled mineralogy)	Alt[c]	$^{87}Sr/^{86}Sr$	[d]N	CO_3[e] min	Mg/Ca (mol)	Sol[f] (wt%)	Ca (wt%)	Mg (wt%)	Sr (ppm)	Fe (ppm)	Mn (ppm)	$\delta^{13}C_{carb}$[g] (‰)	$\delta^{18}O_{carb}$[g] (‰)	$\delta^{13}C_{org}$[g] (‰)	ε_{TOC}[h] (‰)	TOC[i] (wt%)	PIA[j]
T5-04-07a	Werii Slate	899.5	Slate, non-calcareous														-25.88		0.08	88
T3-15-06	Werii Slate	899.5	Slate, non-calcareous																	89
T5-04-07c	Werii Slate	898.0	Slate, non-calcareous																	86
T5-04-06	Werii Slate	853.3	Slate														−28.38		0.11	96
T5-04-05	Werii Slate	794.8	Slate														−28.14		0.08	95
T5-04-04	Werii Slate	771.5	Slate														−27.25		0.08	96
T5-04-03	Werii Slate	748.1	Slate														−26.70		0.15	94
T3-15-04a	Werii Slate	724.7	Slate, varve-like lamina w/minor dolo horizons (dol)	*	0.710439 ± 17	1	D	0.92	11	12.32	6.86	131		2864	4.31	−1.37	−29.26	34.58	0.06	
T3-15-04b	Werii Slate	724.7	Slate w/abundant iron oxide blebs?																	92
T5-04-02	Werii Slate	584.4	Felsic metavolcanics? Flow banded?																	95
T5-04-01	Werii Slate	561.1	Felsic metavolcanic flow agglomerate														−24.63		0.28	69
T3-15-03	Werii Slate	526.0	Slate/metatuff?																	74
T3-15-01	Werii Slate	309.8	Metavolcanics																	45
Negash W. Limb, Madahne Alem																				
T3-11-09	Lower Slate (DF)	296.0	Dolomitic marble	*	0.706470 ± 15	2	D	0.99	87	20.62	12.42	273	1,009	200	2.12	−6.24	−37.73	41.41	0.01	
T3-11-02	Lower Slate (DF)	289.0	Dolomitic marble; possible evap pseudomorphs		0.705191 ± 12	2	D	1.00	99	21.46	13.06	246	2,705	454	3.00	−4.90	−24.13	27.80	0.00	
T3-11-08	Lower Slate (DF)	278.0	Siliceous dolomite, microspar	*	0.706812 ± 20	2	D	0.99	86	22.25	13.33	331	1,769	308	2.74	−6.20	−40.27	44.82	0.02	
T3-11-07	Lower Slate (DF)	258.0	Microbial BS, dolomicrospar/spar		0.705566 ± 19	2	D	0.99	96	23.33	13.99	225	2,301	321	2.53	−5.65	−42.20	46.70	0.06	
T3-11-06	Lower Slate (DF)	249.0	Dolomicrospar; possible evap pseudomorphs		0.705236 ± 20	2	D	1.03	78	22.36	13.91	357	5,277	763	2.59	−4.67	−34.14	38.03	0.04	
T3-11-05	Lower Slate (DF)	239.5	Prismatic sheet crack cement; originally aragonite?	*	0.704763 ± 16	2	D	0.99	89	21.72	13.06	330	5,300	535	2.07	−9.19	−41.75	45.72	0.01	
T3-11-04	Lower Slate (DF)	229.7	Dolomitic marble; possible evap pseudomorphs		0.705246 ± 15	2	D	1.01	88	21.71	13.25	438	3,734	434	1.93	−4.12	−32.72	35.83	0.03	
T5-8-5	Lower Slate (DF)	60.2	Slate																	92
T5-8-4b	Lower Slate (DF)	53.0	Dolomicrospar, possible evap pseudomorphs		0.705005 ± 07	1	D	0.98	100	23.33	13.81	351	5,914	1758	4.60	−3.64	−31.33	37.09	0.04	
T5-8-4a	Lower Slate (DF)	49.0	Slate																	95
T3-11-10	Syntectonic Intrusive	36.0	Metafelsic unit with 774.7 ± 4.8 Ma zircons: possible sill or dike (Avigad et al., 2007), probable metasediment-pebbly sandstone/shale (this study).																	
T5-8-3	Lower Slate (DF)	26.0	Chloritic slate (orange weathering)																	96
T5-8-2	Lower Slate (DF)	14.0	Purple spotted slate																	92

T3-11-03	Lower Slate (DF)	4.0	Grey phyllite																
T3-11-01	Tsaliet Gp, Metavolcs	(6.0)	Polymict metavolcanic conglomerate																87
Negash W. Limb, B–B′																			
T3-10-02	Diamicite (MF)	1632.0	Rounded oolite clast (~10 cm diam)		0.705971 ± 14	2	C	0.08	98	31.64	1.55	512	1,774	1510	0.71	−11.54	−25.21	26.59	0.03	
T3-09-20	Diamicite (MF)	1597.0	Diamictite, matrix supported polymict clasts ≤7 mm																
T3-09-18	Transitional LS (MF)	1436.0	Laminated micropeloidal WS, organic rich		0.706386 ± 14	2	C	0.01	84	41.98	0.31	3922	735	149	5.92	−7.20	−22.55	29.13	0.10	
T3-09-17b	Black LS (MF)	1412.0	MS, DL minor silicified horizons, organic rich	*	0.706409 ± 15	2	C	0.04	69	35.63	0.76	1999	8,337	867	5.16	−10.62	−24.81	30.74	0.12	
T3-09-17	Black LS (MF)	1412.0	MS, DL, organic rich		0.706502 ± 13	2	C	0.01	96	41.50	0.25	2857	80	50	1.42	−4.57	−22.21	24.17	0.11	
T3-09-15	Black LS (MF)	1363.0	MS, DL, external weathering rind alteration	*	0.706655 ± 15	2	C > D	0.23	76	31.60	4.36	1299	11,946	1234	6.70	−3.54	−29.94	37.77	0.09	
T3-09-14	Black LS (MF)	1338.0	MS/WS, cryptic rexld fabric/allochems		0.706712 ± 13	2	C	0.01	89	40.46	0.16	2429	199	66	5.63	−2.43	−20.66	26.84	0.08	
T3-09-13	Black LS (MF)	1314.0	Intraclastic GS		0.706604 ± 15	1	C	0.01	97	39.82	0.14	1848	65	47	6.31	−2.27	−23.27	30.28	0.09	
T3-09-12	Black LS (MF)	1289.0	MS, DL		na		C	0.01	95	40.24	0.19	2,697	147	34	6.35	−3.36	−20.89	27.82	0.11	
T3-09-11	Black LS (MF)	1264.0	Intraclastic? WS, IL, organic rich, cryptic clasts		0.706514 ± 13	2	C	0.01	97	35.43	0.16	2430	65	46	5.84	−3.11	−22.24	28.72	0.10	
T3-09-10	Black LS (MF)	1240.0	Intraclastic? WS, IL, organic rich, cryptic clasts		0.706574 ± 13	2	C	0.01	98	38.94	0.18	2457	76	29	4.29	−5.14	−22.90	27.83	0.10	
T3-09-09	Black LS (MF)	1216.0	Layered MS, organic rich		0.706593 ± 12	2	C	0.06	97	32.25	1.24	442	1,066	209	1.41	−1.15	−24.52	26.58	0.09	
T3-09-08	Dol>Slate (DF)	1166.0	Dolomicrospar/spar		0.706150 ± 13	2	D	0.98	96	20.74	12.32	164	249	113	−2.26	−4.98	−29.41	27.98	0.01	
T3-09-07	Dol>Slate (DF)	808.0	Dolomite w/evap pseudomorphs, DL		0.706206 ± 13	2	D	0.99	97	23.06	13.81	283	3,038	334	3.50	−5.03	−34.82	39.70	0.02	
T3-09-06	Slate>Dol (DF)	515.0	Dolomite w/evap pseudomorphs, DL		0.705922 ± 23	2	D	1.07	93	18.53	12.08	518	1,855	242	3.76	−4.25				
T3-09-05	Slate>Dol (DF)	477.0	Graphitic slate/phyllite																	96
T3-09-04	Slate>Dol (DF)	467.0	Graphitic slate																	
T3-09-03	Slate>Dol (DF)	456.0	Slate/phyllite																	
T3-09-02	Slate>Dol (DF)	445.0	Dolomite w/evap pseudomorphs, DL		0.705524 ± 15	2	D	0.99	86	21.73	13.07	455	3,301	783	3.44	−4.77	−41.40	46.78	0.01	
T3-09-01	Slate>Dol (DF)	435.0	Dolomite w/evap pseudomorphs, DL		0.705598 ± 16	2	D	0.98	97	23.09	13.70	565	2,925	743						
Negash E. Limb																				
T4-33-14	Dol>Slate (DF)	1113.0	Laminated dolomicrospar						96						−0.15	−4.20	−25.21	25.71	0.01	
T4-33-13	Dol>Slate (DF)	1088.0	Siliceous dolomite, faintly layered						96						−1.71	−5.15	−31.72	30.99	0.01	
T4-33-12	Dol>Slate (DF)	1062.0	Dolomitic marble						97						−1.70	−3.71	−27.19	26.20	0.01	
T4-33-10	Dol>Slate (DF)	932.0	IL dolomicrospar, weathered						49						−0.43	−4.99	−26.48	26.76	0.07	
T4-33-08	Dol>Slate (DF)	809.0	Slate, green														−26.79		0.12	96
T4-33-07	Dol>Slate (DF)	715.0	Dolomicrospar, faintly layered						91						−1.74	−4.29	−24.75	23.59	0.04	
T4-33-06	Dol>Slate (DF)	676.0	Dolomicrospar, finely layered						77						−2.58	−4.41	−26.84	24.93	0.04	
T4-33-04B	Dol>Slate (DF)	516.0	Dolomicrospar						74						−1.93	−2.17	−29.82	28.75	0.19	

Table 1 (*Continued*)

Transect/sample ID	Unit	Height[a] (m)	Sample description[b] (microdrilled mineralogy)	Alt[c]	$^{87}Sr/^{86}Sr$	[d]N	CO_3[e] min	Mg/Ca (mol)	Sol[f] (wt%)	Ca (wt%)	Mg (wt%)	Sr (ppm)	Fe (ppm)	Mn (ppm)	$\delta^{13}C_{carb}$[g] (‰)	$\delta^{18}O_{carb}$[g] (‰)	$\delta^{13}C_{org}$[g] (‰)	ε_{TOC}[h] (‰)	TOC[i] (wt%)	PIA[j]
Negash W. Limb, A–A′																				
T3-07-01	"Mareb" Granitoid		Granite (did not yield suitable zircons for geochronology)																	
T3-06-11	Slate>Dol (DF)	403.0	Dolospar marble w/evap pseudomorphs		0.706042 ± 13	2	D	0.99	97	21.51	12.87	413	889	127	2.91	−3.80				
T3-06-10	Slate>Dol (DF)	389.0	Dolospar marble w/evap pseudomorphs	*	0.706231 ± 12	2	D	0.99	94	23.43	14.04	290	2,501	226	2.84	−3.97	−39.29	43.86	0.02	
T3-06-09	Slate>Dol (DF)	375.0	Grey phyllite																	92
T3-06-07	Slate>Dol (DF)	348.0	Slate/green phylllite; chloritic?																	
T3-06-06	Slate>Dol (DF)	335.0	Dolomicrospar w/evap pseudomorphs	*	0.705357 ± 16	2	D	1.02	88	22.20	13.67	484	7,888	1033	2.23	−4.89	−32.50	35.90	0.03	
T3-06-05	Slate>Dol (DF)	321.0	Layered dolomicrospar w/evap pseudomorphs	*	0.705251 ± 14	2	D	1.02	86	22.58	13.90	429	3,851	620	3.06	−4.96	−31.19	35.35	0.01	
T3-06-04	Slate>Dol (DF)	308.0	Layered dolomicrospar w/evap pseudomorphs	*	0.704969 ± 11	2	D	1.02	83	22.75	14.10	700	4,907	666	2.36	−6.02	−37.53	41.45	0.02	
T3-06-03	Slate>Dol (DF)	287.0	Slate																	96
Samre area																				
T3-30-9b	Didikama Fm?	1100.0	MS/Micropeloidal WS (NFC)		0.705327 ± 26	2	C	0.01	89	64.29	0.38	267	412	65	4.11	−1.94	−26.39	31.32	0.07	
T3-30-9b	Didikama Fm?	1100.0	Dolomitized prismatic sheet crack cement (dol)		0.705582 ± 18	2	D	0.99	90	21.07	12.60	1,885	6,367	224	2.86	−5.97				
T3-30-9	Didikama Fm?	1099.0	IL micropeloidal GS/PS; dolomitized	*	0.706336 ± 19	2	D	4.49	48	8.57	23.31	255	21,806	889	3.06	−2.37	−24.87	28.65	0.08	
T3-30-15	Didikama Fm?	1043.0	Slate																	
T3-30-8	Didikama Fm?	1025.0	Dolomicrospar, cryptic primary fabric		0.705787 ± 19	2	D	0.95	81	22.35	12.92	402	4,078	1365	1.77	−1.77	−28.00	30.63	0.03	
T3-30-5b	Didikama Fm?	868.0	Dolomicrospar and spar, rexld primary fabric	*	0.704984 ± 17	2	D	0.99	99	16.07	9.66	2,078	3,644	515	5.73	−11.88	−28.82	35.57	0.00	
T3-30-5a	Tsaliet Gp - Metavolcs	856.0	Serpentinite?																	
T3-30-3	Tsaliet Gp—Metavolcs	486.0	Microspar, cryptic primary fabric	*	0.704694 ± 17	2	C	0.00	79	42.83	0.12	512	521	860	2.99	−7.09	−26.69	30.50	0.02	

[a] Stratigraphic height above base of Tambien Group as defined in Beyth (1972); Samre area datums relative to base of transect.

[b] BS = boundstone, DL = diffusely layered, Dol = dolomite, Dolo = dolomitic, evap = evaporite, FC = ferroan calcite "blue" fabric, GS = grainstone, IL = Irregularly layered, MS = mudstone, NFC = non-ferroan "pink" fabric, PS = packstone, WS = wackestone.

[c] Samples interpreted as having most altered $^{87}Sr/^{86}Sr$.

[d] Number of sample runs averaged for reported $^{87}Sr/^{86}Sr$.

[e] Carbonate mineralogy inferred from molar Mg/Ca with cut-offs of 0.15, 0.50, and 0.85 separating calcite (C), calcitic (C > D), dolomitic (D > C), and dolomite (D).

[f] wt% of sample soluble in 0.8 M acetic acid.

[g] Relative to the PDB belemnite standard.

[h] ε_{TOC}* (‰) is essentially the fractionation between inorganic and organic carbon = 10^3 ($\alpha_{TOC} - 1$) = 10^3 $\{[(\delta^{13}C_{carb} + 1000)/(\delta^{13}C_{org} + 1000)] - 1\} \approx \delta^{13}C_{carb} - \delta^{13}C_{org}$ (Hayes et al., 1999).

[i] wt% total organic carbon in the rock.

[j] PIA is the plagioclase index of alteration = $100 \times [(Al_2O_3 - K_2O)/(Al_2O_3 + CaO + Na_2O + K_2O)$, where CaO* is for silicate-bearing minerals only (Fedo et al., 1995). Scores range from 50 to 100, respectively for unweathered and extremely weathered rock.

culminating with black limestone and diamictite of the Matheos Formation.

3.4. Samre area (Area D)

Tigre's southernmost Neoproterozoic metasediments outcrop in the Samre region, 90 km SW of Negash. We investigated this area as a possible southern continuation of the Negash synclinorial trend (Fig. 4D) that might preserve metasediments younger than the Negash diamictite. The Samre region has not been mapped in detail, and our investigations were limited to reconnaissance. The Tambien Group is undifferentiated on the Mekele sheet map (Arkin et al., 1971) but includes NNE-trending carbonate units. Analysis of satellite imagery following our field investigations suggests that the regional structure may be a NNE-plunging synclinorium, with our sampling transect involving only the lower portion of the NW structural limb (Fig. 4D). Here we encountered lithologies consistent with the transition from Tsaliet Group metavolcanics to basal Tambien Group (Didikama Formation) deposition. The synclinorial fold axis appears to be ~3 km further SE from the stratigraphically highest transect locality (Fig. 4D). A distinctive, dark, ridge-forming unit rims the inner portion of this structure and, based on comparison with Negash synclinorium (field transects and satellite imagery), may be equivalent to the Matheos Formation Black Limestone (*cf.* Fig. 4C).

4. Methods

4.1. Field collection

Sample localities were photographed, georeferenced (GPS), and described for principal field characteristics (attitude, lithology, bedding aspect, primary depositional and secondary alteration features). We collected fresh limestone and dolomite with primary depositional textures as marine proxy record candidates, and intercalated slates to investigate chemical weathering trends. The sample data set presented here (Table 1) consists of 100 carbonate and 30 slate intervals.

4.2. Petrography and microsampling

Samples were slabbed perpendicular to bedding and thin sections (half stained with Alizaren Red-S and potassium ferricyanide) and corresponding polished blanks were prepared. During petrographic description, optimal target phases for geochemistry were microsampled using a carbide dental burr from razed, impurity-free, surfaces on corresponding polished blanks. Harvested powders were typically 5 mg for C and O isotopes and 15 mg (total) for Sr isotopes and ICP analysis. The burr was acid-cleaned (1 M HOAc) and inspected to be carbonate free between samplings. Carbonate mud, peloids, intraclasts, and oncoids, and their diagenetic equivalents (mainly as microspar fabrics) are predominant constituents in Tambien carbonates and in most cases it was not possible to sample discrete allochems. Slab areas retaining primary depositional textures or homogeneous microsparry areas free of secondary features (*e.g.*, fractures/cements, stylolites, weathering rinds) were preferentially targeted. Silicate (quartz and less commonly authigenic feldspar) cement was a common minor authigenic component of Didikama Formation dolomites that could not be entirely avoided during sampling. Late carbonate cements and secondary alteration fabrics were also occasionally sampled to assess possible diagenetic pathways.

4.3. Elemental and isotopic analysis

Samples were fully reacted with 0.8 M HOAc (in loosely capped sterile microvials constantly agitated by inclined rotation), centrifuged, and leachates subsampled for ICP-OES and Sr isotopes. Insoluble residues, acid-neutralized by repeated centrifuge-washing with deionized water, were dried and weighed to determine the acid-soluble carbonate (ASC) content. The acid strength and volumes used typically provided less than a twofold molar excess above that required for total carbonate dissolution. Given that acetic acid is a weak acid (only partially dissociated in water) and the high carbonate content of most samples (median: 87%), dissolution of low-solubility non-carbonate phases was unlikely. Leachate aliquots for ICP-OES were diluted in 4% HNO_3 to present a typical net dilution factor of 2300 ± 500, and major and minor cation contents determined on a Perkin Elmer Optima 3300DV plasma emission spectrophotometer (Geosciences Dept., Univ. of Texas at Dallas) from linear portions of intensity versus concentration calibration curves established from measurement of calibration solutions. Systematic measurement of a multi-element calibration standard was used to check and compensate for analytical drift in the intensity-concentration normalization baseline.

Leachate Sr was extracted by standard procedures using Sr-specific resin (EIChromM Sr Resin SPS) and isotopic compositions determined using Finnigan MAT-261 variable collector thermal ionization mass spectrometers at the University of Texas at Dallas (static measurement) and University of Texas at Austin (dynamic measurement). Static mode analyses were performed in two intensive analytical sessions (each spanning several weeks, with replicate analyses of samples) over a 2-year interval, whereas dynamic mode analyses were made during a single analytical session (2 weeks). Isotopic measurements typically involved 160 multicollection cycles of all four Sr isotopes in addition to ^{85}Rb, for monitoring ^{87}Rb, while maintaining the $^{88}Sr^{+}$ ion beam at 3.5 ± 0.5 V (static) and 5.5 ± 0.5 V (dynamic) on a 10^{-11} Ω resistor. To correct for mass discrimination during evaporation and ionization, Sr isotopic ratios were normalized to $^{86}Sr/^{88}Sr = 0.1194$ using a linear correction scheme. NIST SRM-987, analyzed at least once before and after daily sample runs, averaged 0.710253 ($n = 73$) for all static mode runs and 0.710239 ($n = 13$) for dynamic runs. Precision on standards and replicates during each analytical session was better than 25 ppm (static mode) and 16 ppm (dynamic mode). For consistency and to aid in comparisons with other studies, reported $^{87}Sr/^{86}Sr$ results are normalized to a consistent baseline of 0.710240 for SRM-987. A weighted mean of modern seawater $^{87}Sr/^{86}Sr = 0.709180 \pm 0.000011$ is inferred from 11 static mode measurements of modern carbonate standard EN-1.

C and O isotopes and TOC were measured at the Geological Survey of Israel. Carbonate $\delta^{18}O$ and $\delta^{13}C$ were determined using a VG ISOCARB system coupled to a SIRA-II mass spectrometer (Shackleton, 1974). In the Isocarb, samples were reacted successively under vacuum in a common-bath reservoir of ~100% orthophosphoric acid (H_3PO_4) at 90 °C. Calibration of the mass spectrometer to the international Pee Dee Belemnite (PDB) carbonate standard was derived via National Bureau of Standards (NBS) 19 following Coplen (1988). Instrument precision was better than ± 0.1‰ for both $\delta^{13}C$ and $\delta^{18}O$, and external reproducibility was ≤0.05‰ based on duplicate reference standard measurements. In preparation for $\delta^{13}C$ measurement of the associated organic fraction ($\delta^{13}C_{org}$), pulverized samples were repeatedly pretreated with dilute hydrochloric acid (0.1N HCl) at 50 °C to remove all carbonate phases, neutralized by repeated centrifuge-washing with distilled water, and oven-dried at 50 °C. TOC and $\delta^{13}C_{org}$ values were then determined after combustion at ~1750 °C in an elemental analyzer (EA-1112) unit connected online via a Conflo-III interface to a ThermoFinnigan Delta-Plus XP mass-spectrometer. USGS-24 (graphite: $\delta^{13}C = -15.99$‰) was used to calibrate measurements to the PDB scale (Craig, 1957). The TOC content was calibrated using international standards SO-1 and SCO-1 (0.27% and 0.81%, respectively). Analytical precision of TOC and $\delta^{13}C_{org}$ values was ± 0.1%

and ± 0.1‰, respectively. All isotope ratios are expressed as per mil (‰) variations from the V-PDB international standard.

4.4. Chemical index of weathering

Slate (Werii Slate, Lower Slate of the Didikama Formation) billets were cleaned of external contaminants (saw marks) and pulverized. Sample splits were analyzed by XRD to screen for carbonate phases and XRF (Activation Labs, Ontario) to determine major element oxides. The ratio of immobile to mobile elements was calculated as the Plagioclase Index of Alteration (PIA, Fedo et al., 1995) according to

$$\mathrm{PIA} = \frac{100 \times (\mathrm{Al_2O_3} - \mathrm{K_2O})}{\mathrm{Al_2O_3} + \mathrm{CaO^*} + \mathrm{Na_2O} - \mathrm{K_2O}}$$

where CaO* refers only to silicate-bearing minerals. This index monitors the extent of plagioclase weathering. Scores range from 50 for fresh rocks to 100 for extremely weathered rocks; essentially fully converted to clay. Although we obtained similar results using other weathering indices (*i.e.*, CIA of Nesbitt and Young, 1982), we consider the PIA to be a superior weathering proxy for low-grade metasediments because it minimizes potential bias associated with potassium metasomatism.

5. Diagenetic considerations

The objectives of diagenetic sample screening are to gauge the compositional influences of various diagenetic pathways that could overprint primary marine signatures. Our localities are structural folds within the Pan African orogenic belt, which appear to have only experienced low-grade metamorphism. Low-grade (<250 °C) metamorphism of high purity Tambien Group carbonates is unlikely to disturb primary C and Sr isotope ratios, unless high to very high water:rock ratios are involved (Alene et al., 2006). The purest carbonate units sampled in our study have median ASC contents exceeding 95%, and the average for the entire study exceeds 93% (n = 94). In view of the conservative (weak acid) leachate used, ASC contents are likely somewhat higher. Given the abundance of microspar in the Tambien Group, including distinctive Sr-rich units, it is reasonable to infer an abundance of micrite-rich depositional settings with inherently low early diagenetic permeabilities that would favor largely closed-system diagenesis and retention of primary Sr concentrations and isotopic compositions. Nonetheless, neomorphism, dolomitization, pressure solution, and other diagenetic processes have led to minor chemical alteration in Tambien Group carbonates.

5.1. $\delta^{18}O_{carb}$

The primary $\delta^{18}O$ composition of marine carbonate is the product of isotopic fractionation with water oxygen at ambient equilibrium conditions of temperature, salinity, and pH (Jaffrés et al., 2007). Carbonates are systematically enriched in ^{18}O compared to parent seawater, with the magnitude of variation related to temperature and associated physicochemical conditions (Kasting et al., 2006). Because of the high content of O compared to C and Sr in most diagenetic fluids, $\delta^{18}O_{carb}$ is the isotopic system most susceptible to fluid-rock overprinting (Banner and Hanson, 1990; Jacobsen and Kaufman, 1999). The extent that this proxy mimics secular changes in contemporaneous seawater supports that Sr- and C-isotopic compositions should be preserved. Such comparisons require accurate knowledge of ancient marine secular $\delta^{18}O$ variation, as is reasonably well constrained for Mesozoic and Cenozoic oceans. However, the Cryogenian $\delta^{18}O$ record is uncertain because (1) glacial-interglacial oscillations should have been associated with high amplitude $\delta^{18}O$ variations that may not be unambiguously differentiable between sequences, and (2) the lack of well-dated and well-preserved reference records precludes an empirical basis for assessing sample preservation. Documented pre-"Sturtian" $\delta^{18}O_{carb}$ variations are mainly between −5 and −11‰ for samples judged to retain near-pristine $\delta^{13}C$ and/or $^{87}Sr/^{86}Sr$ depositional signatures (Jacobsen and Kaufman, 1999, their Fig. 6; supplementary information in Halverson et al., 2005). Most (85%) of our Tambien samples fall within this range. Tambien Group post-deformational calcite vein cements are generally lighter (range: −20.6 to −7.9‰, n = 5) than adjacent limestones, suggesting the influence of low $\delta^{18}O$ meteoric or metamorphic fluids (Alene et al., 2006). However, as absolute rock-vein variations are minor (within 1.2‰, n = 4), water/rock ratios were likely low and/or exchange was kinetically limited (Alene et al., 2006). Because samples most overtly altered by rock/fluid interaction are likely to have $\delta^{18}O$ lower than the initial sediment (Jaffrés et al., 2007), caution is warranted for samples lighter than the modal range of Cryogenian samples; namely < -11‰, a limit suggested by Kaufman et al. (1993). Fourteen samples in our data set exceed this cut-off, but only to an extreme of −13.2‰. Most derive from basal Tambien Group carbonates in the Shiraro Area (n = 6) and in Mai Kenetal (n = 5) synclinorium. An additional consideration for interpreting $\delta^{18}O$ signatures is that dolomites are estimated to be 3–4‰ heavier than precursor calcite due to equilibrium fractionation processes (Land, 1980), as consistent with the observation that dolomites are typically enriched by 2–4‰ compared to coeval limestone (Jaffrés et al., 2007, and references therein). Samples from the dolomitic upper Didikama Formation (Negash) are 4–5‰ heavier than the prospectively equivalent (based on negative $\delta^{13}C$, see Section 7.1) Assem Limestone (Mai Kenetal); partially dolomitized Assem Limestone samples also have enriched $\delta^{18}O$ compositions that could be consistent with this effect.

5.2. $^{87}Sr/^{86}Sr$

Tambien carbonates are not primary phases, but were finely recrystallized during diagenesis and/or low-grade metamorphism. Overprinting of primary $^{87}Sr/^{86}Sr$ compositions may result from the addition of foreign (non-marine and/or non-contemporaneous marine) Sr during early diagenesis or greenschist metamorphism. Contamination sources may be internal (*e.g.*, alteration of siliciclastic detritus or radiogenic ingrowth from ^{87}Rb) or external (from fluid flow, either channelized or diffusive), and more or less radiogenic than the original marine signature. However, as earlier posited, low porosity-low permeability micrite-dominated carbonate facies may have been effectively buffered from significant fluid/rock interactions, and such "closed systems" would favor retention of marine $^{87}Sr/^{86}Sr$ signatures.

Many diagenetic tracers (*e.g.*, [Sr], [Mn], [Fe], Mn/Sr, Fe/Sr) used to identify samples with least-altered $^{87}Sr/^{86}Sr$ originate from fluid/rock modeling studies, particularly as applied to meteoric and marine diagenesis (and dolomitization). Such alteration processes typically involve loss of Sr and addition of elements such as Mn and Fe, and therefore potentially also foreign Sr (Brand and Veizer, 1980; Derry et al., 1992). The predicted result of diagenetic overprinting is a significant change in $^{87}Sr/^{86}Sr$ below some threshold [Sr] (Banner and Hanson, 1990; Jacobsen and Kaufman, 1999). This effect is most apparent for low-Sr carbonates, depending on initial carbonate composition, water:rock ratio, and types of diagenetic fluids (Halverson et al., 2007). In cratonic platform settings, diagenesis generally increases $^{87}Sr/^{86}Sr$ because weathering of continental crust and sediments provides a flux of dissolved radiogenic Sr and/or Rb to diagenetic fluids. The opposite influence, toward unradiogenic $^{87}Sr/^{86}Sr$, is expected for weathering of ensimatic materials. Various Mn/Sr (and Fe/Sr) tolerances have been proposed for culling least altered $^{87}Sr/^{86}Sr$ compositions,

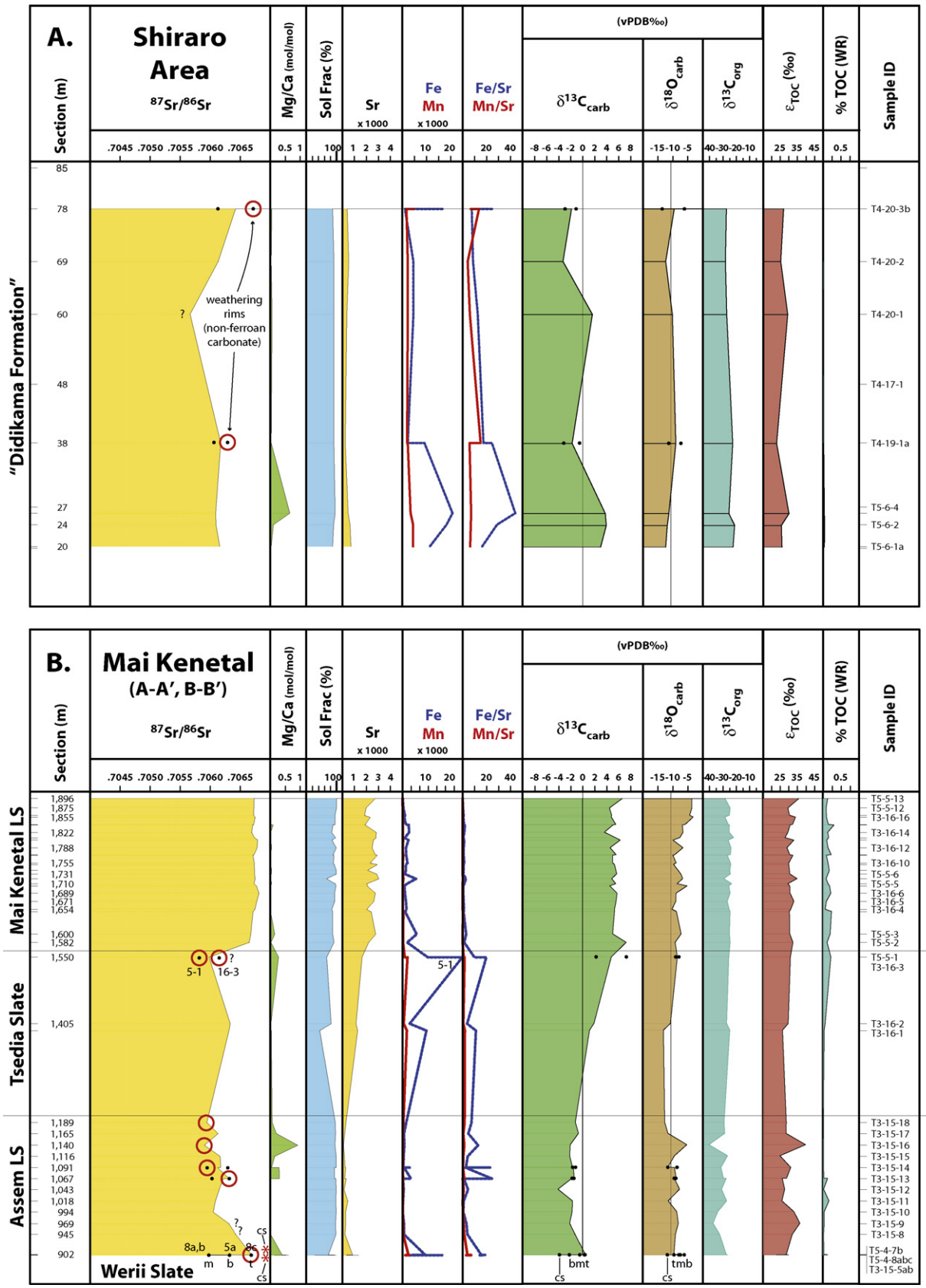

Fig. 6. Composite chemostratigraphic logs for Tambien Group transects. With the exception of extreme $^{87}Sr/^{86}Sr$ outliers (*), curves are the running stratigraphic average of all analyses (*cf.* Table 2); individual data points are preserved for horizons containing multiple analyses. Samples judged to be altered for $^{87}Sr/^{86}Sr$ are circled in red. (A) Shiraro area carbonate ridges (W. Tigre). (B) Combined Mai Kenetal transects A–A′ and B–B′. The basal dolomite unit of the Assem Limestone is least radiogenic near its center (m) compared to its upper (t) and lower (b) margins and bounding calcareous slate (cs). (C2) Combined Negash west limb transects A-A′ and B-B′. C and O isotope data for the Didikama Formation are supplemented by seven samples (connected by dashed horizontal lines) from the eastern synclinorial limb. (C1) Basal Tambien Group carbonate exposures at Madahne Alem. (D) Lower Tambien Group (Didikama Formation) exposures for Samre area (S. Tigre).

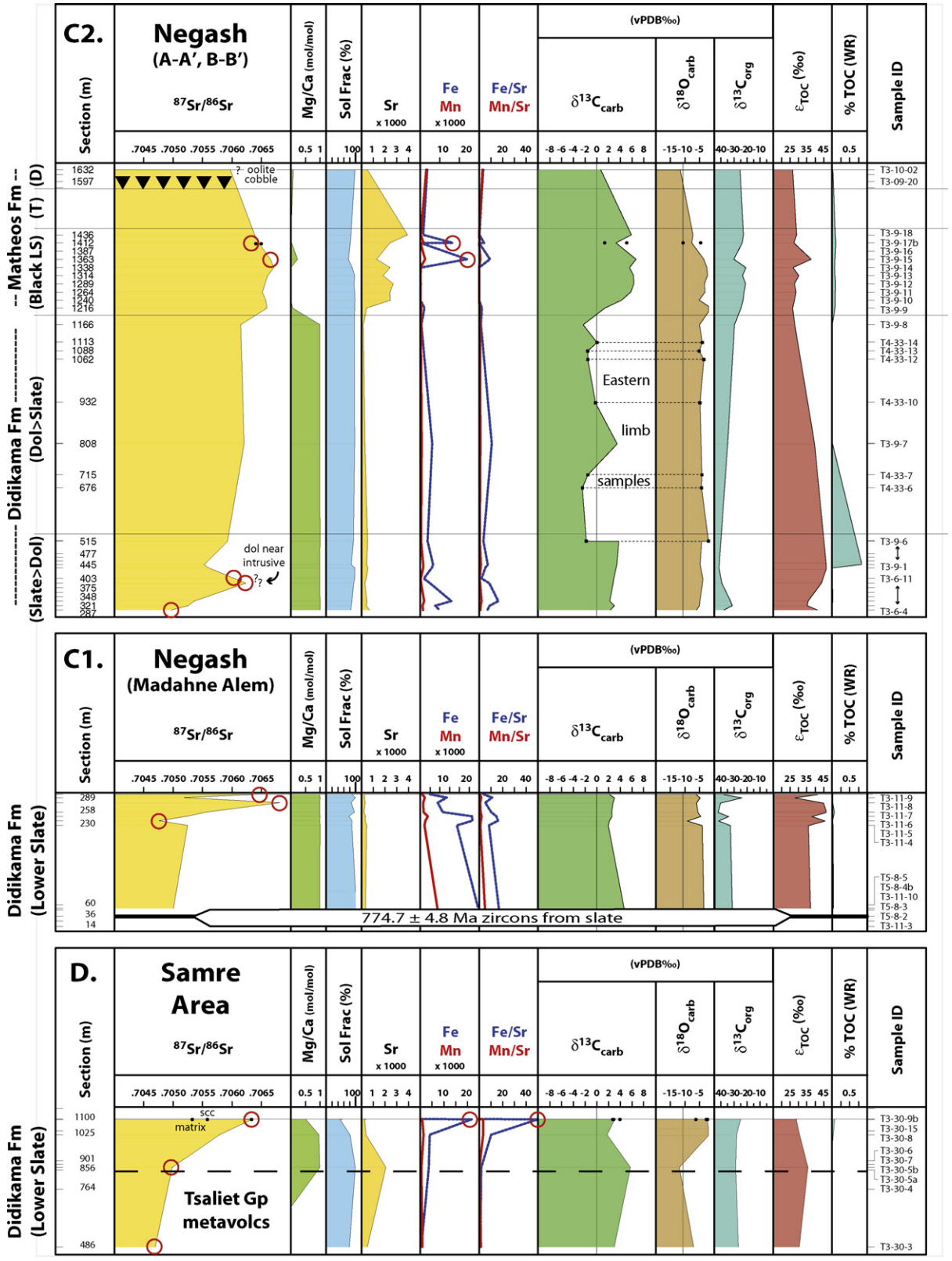

Fig. 6. (*Continued*).

but the fact that these range over two orders of magnitude for samples judged to retain primary $^{87}Sr/^{86}Sr$ and/or $\delta^{13}C_{carb}$ argues against any universal value (<0.2: Misi and Veizer, 1998; Fairchild et al., 2000; <2: Kaufman and Knoll, 1995; <10: Knoll et al., 1995). The redox character of Cryogenian oceans and associated carbonate depositional environments may also limit the utility of such indices. The limited resurgence of BIFs, and iron-enriched mudstones and carbonates in association with Cryogenian glacigenic deposits (Kirschvink, 1992; Hoffman and Schrag, 2002; Canfield et al., 2007) suggests at least regional development of anoxic condi-

tions, and a significantly dampened influx of sulfate to oceans is predicted as a consequence of widespread continental glaciation and a diminished hydrologic cycle (Canfield and Raiswell, 1999; Hoffman, 2004). Furthermore, Neoproterozoic sulfur isotope surveys suggest that pre-Marinoan oceans had few oxidants (Hurtgen et al., 2005). Without abundant oxygen and sulfate, dissolved concentrations of redox sensitive elements like Mn and Fe would have been substantially higher than modern oceans (Anbar and Knoll, 2002) and may have co-precipitated with carbonates. Microbially induced carbonate production in anoxic early diagenetic porewaters might obtain a similar result.

Dolomites generally have a poor reputation for preserving primary $^{87}Sr/^{86}Sr$ (Fairchild and Kennedy, 2007). Dolomitization (the conversion of calcium carbonate minerals to dolomite, or replacement thereof) is the traditional interpretation for dolomite genesis. This process requires extensive fluid-rock interaction (to exchange Ca for Mg; Land, 1973) that lowers Sr concentration from that in precursor mineralogy and potentially incorporates foreign Sr. Thus, low-Sr dolomites warrant appropriate scrutiny. For example, Halverson et al. (2007) found most low-Sr (122 ppm avg) dolomites to be more radiogenic compared to stratigraphically equivalent or proximal limestones. However, there is growing evidence that benthic microbial communities may, via anoxic diagenesis, play a direct syn-sedimentary role in dolomite formation (Wright and Oren, 2005), and limited support that such early diagenetic phases can preserve near primary marine $^{87}Sr/^{86}Sr$ (Baker, 1990; Miller, 1990; Bernoulli et al., 2004). Proterozoic dolomite formation was commonly syngenetic involving fluids isotopically similar (at least with regard to $\delta^{13}C$) to seawater (Kaufman and Knoll, 1995). Common observation of penecontemporaneous cements associated with some dolostones suggests that these became closed systems during early diagenesis, and therefore may have resisted overprinting by later diagenetic fluids (Tucker, 1983; Fairchild and Spiro, 1987). For such reasons, mineralogy alone is not a compelling reason to reject $^{87}Sr/^{86}Sr$ signatures of Tambien Group dolomites. We note that most Tambien dolomites ($Mg/Ca_{mol} \geq 0.9$) have relatively high Sr contents (avg = 363 ± 148 ppm; n = 22), similar to those reported for Neogene organogenic dolomite (*e.g.*, 300-500 ppm, or higher: Burns and Baker, 1987; Burns et al., 1988; Miller, 1995; Malone et al., 1996, Mazzullo, 2000) and equal to or higher than some well-studied Neoproterozoic limestones (*e.g.*, Asmerom et al., 1991; Kaufman et al., 2006), suggesting that they have not lost substantial Sr. These observations indicate that although several logical alteration proxies can be postulated, none are *a priori* evidence of $^{87}Sr/^{86}Sr$ disturbance. We feel that the best evidence for preservation of primary $^{87}Sr/^{86}Sr$ is the extent to which stratigraphic-trends can be demonstrated and outliers explained by various geochemical proxies in conjunction with sample appearance, particularly for rocks that preserve reasonable $\delta^{13}C_{carb}$ compositions. We concur with Halverson et al. (2007) that geochemical alteration criterion are best established empirically, by region and/or lithological unit, on a case-by-case basis. Robust results using this approach require adequate stratigraphic sampling, and modestly sampled continua must be interpreted cautiously.

Incorporation of Rb in fluids is potentially significant for affecting $^{87}Sr/^{86}Sr$ in Neoproterozoic rocks. As an example, a limestone with 2000 ppm Sr that incorporates 1 ppm Rb during early diagenesis would increase its $^{87}Sr/^{86}Sr$ by 0.000014 (equivalent to in-run analytical precision) within a period of 700 myrs. Our samples were consistently below Rb detection limits by ICP-OES, which equates to worst-case Rb concentrations of 5 ppm. Although this screening does not exclude radiogenic ingrowth of ^{87}Sr from low Rb/Sr carbonate, we see no systematic correlation between $^{87}Sr/^{86}Sr$ and samples with high ASC contents (>70%). Many authors have argued that ingrowth is unlikely to significantly affect Sr-rich limestones (Derry et al., 1989: 200–2500 ppm; Asmerom et al., 1991: 100–500 ppm (dol: 30–60 ppm); Kaufman et al., 1993: 37–3705 ppm, with negligible measured vs. intial $^{87}Sr/^{86}Sr$ variation when >1000 ppm). Upper Tambien Group black limestones (Matheos Formation, Tsedia Slate, Mai Kenetal Limestone) have comparable or higher Sr contents ranging up to 3922 ppm (typically 1500–3000 ppm). Median Sr concentrations for dolomites (~23% of the study collection) and limestones are 354 ± 148 ppm and 1799 ± 1055 ppm, respectively.

The stratigraphic and structural setting of Tambien Group carbonates allows meteoric and diagenetic fluid $^{87}Sr/^{86}Sr$ compositions to be partially predicted. The Nakfa terrane is juvenile Neoproterozoic crust dominated by lower Rb/Sr rocks (Teklay et al., 2001; Sifeta et al., 2005) so fluids equilibrated with its weathered equivalents should be dominantly characterized by unradiogenic Sr. Tambien carbonates deposited on such a landscape could be susceptible to early diagenetic fluids bearing unradiogenic Sr, but this potential should have progressively dampened as older crust subsided and deposition of marine chemical sediments proceeded. As a result of Late Neoproterozoic deformation, our localities now generally lie within synclinoria flanked by highlands of Tsaliet Group metavolcanics. Metamorphism and recent weathering of this landscape could provide a flux of unradiogenic Sr to meteoric fluids. Thus, late cements originating from meteoric fluids might have lower $^{87}Sr/^{86}Sr$ than unaltered host carbonate. However this flux would be buffered by higher solubilities of any carbonates in the flow path. Our composite $^{87}Sr/^{86}Sr$ data set is mostly consistent with the documented range of pre-"Sturtian" Cryogenian data (*c.* 0.7052–0.7070; Melezhik et al., 2001), but the fact that least radiogenic samples tend to occur in samples with <700 ppm Sr and <90% ASC could mean that such samples are altered.

5.3. $\delta^{13}C_{carb}$ and $\delta^{13}C_{org}$

Assuming equilibrium precipitation, the primary $\delta^{13}C_{carb}$ composition is a proxy for dissolved marine CO_2 ($\delta^{13}C_{DIC}$). Owing to the lack of significant carbon in meteoric and diagenetic fluids compared to concentrations in carbonate rocks or sediments, $\delta^{13}C_{carb}$ and $\delta^{13}C_{org}$ are less susceptible to diagenetic exchange compared with $^{87}Sr/^{86}Sr$ or $\delta^{18}O$. This is often the case even in diagenetically altered or dolomitized carbonates (Tucker, 1983, 1985; Knoll et al., 1986; Fairchild and Spiro, 1987; Burdett et al., 1990; Kaufman et al., 1991; Narbonne et al., 1994; as in Kaufman and Knoll, 1995), despite the fact that dolomite in equilibrium with calcite can be enriched in $\delta^{13}C$ by ~2‰ (Sheppard and Schwarcz, 1970). Unlike its O-isotope equivalent, such C-isotope fractionation is seldom observed in rocks (Hayes et al., 1999; Shields and Veizer, 2002), possibly due to inheritance by dolomites of precursor C or different C fractionation pathways associated with benthic microbial dolomite formation.

Overprinting of the original carbon isotopic composition of carbonates occurs by re-equilibration with fluids of contrasting isotopic composition. This may occur in several ways such as neomorphism (recrystallization, inversion), addition of isotopically distinct carbonate to the diagenetic system, or by metamorphic decarbonation reactions in the presence of siliciclastic materials (Kaufman and Knoll, 1995). The low thermal regime associated with Tambien Group metasediments suggests that metamorphic decarbonation reactions are unlikely, the predicted effect of which would be to release isotopically light volatiles to diagenetic/metamorphic fluids thereby enriching residual $\delta^{13}C_{org}$ (Schidlowski, 1987; DesMarais et al., 1992; Kaufman and Knoll, 1995). Some studies show that isotopic overprinting of $\delta^{13}C$ occurs during late diagenetic neomorphism, provided sufficient permeability and access to meteoric fluids (Fairchild et al., 1990; Beeunas and Knauth, 1985). Most of the previously discussed proxies for evaluating preservation of the $\delta^{18}O$ and $^{87}Sr/^{86}Sr$ signature in

carbonates also hold for $\delta^{13}C$. Because diagenetic introduction of allogenic species may result in congruency, lack of covariance among these proxies (*i.e.*, $\delta^{18}O$ vs. $\delta^{13}C$; $\delta^{18}O$ vs. Mn/Sr; $\delta^{18}O$ vs. $^{87}Sr/^{86}Sr$; $\delta^{18}O$ vs. Mg/Ca) is often cited as consistent with preservation.

Microbial degradation of organic matter produces byproducts with distinct $\delta^{13}C$ compositions and is the most likely mechanism for diagenetic overprinting of marine $\delta^{13}C$ signatures (Kaufman and Knoll, 1995). Organic matter may originate via photosynthesis, sulfate reduction, or methanogenesis. Photosynthetic organic matter is strongly depleted in $\delta^{13}C$ relative to carbonate precipitated from the same parcel of water. Its subsequent degradation via oxidation (fermentation) or methanogenesis produces isotopically light CO_2, which fosters precipitation of isotopically light diagenetic carbonate. Methanogenic degradation of organic matter can supply isotopically heavy CO_2 to porewaters, if extremely light-fractionated methane escapes early diagenesis. Subsequent precipitation of diagenetic carbonate may be heavier than the original seawater composition. Thermogenic breakdown of organic matter may have similar consequences. A maximum 3‰ positive shift in $\delta^{13}C_{org}$ is predicted for thermal maturation of organic matter to kerogen or graphite (Schidlowski, 1987; Alene et al., 2006). Correlation between TOC content and $\delta^{13}C_{org}$ or ε_{TOC} (Hayes et al., 1999; next paragraph) may indicate such an effect.

Hayes et al. (1999) compiled estimated average isotopic compositions for Neoproterozoic marine carbonates ($\delta^{13}C_{carb}$) and sedimentary organic material ($\delta^{13}C_{org}$), and their absolute difference (ε_{TOC}). This comparison indicates that isotopic fractionation (ε_{TOC}), between carbonate and TOC reservoirs, oscillated over a 10‰ range (24–34‰) throughout the Neoproterozoic but was mutually consistent over shorter time intervals. A consistent offset between $\delta^{13}C_{carb}$ and $\delta^{13}C_{org}$ (typically in the range of ~28.5‰, Knoll et al., 1986) is often considered to indicate preservation of marine $\delta^{13}C_{carb}$. This reasoning applies to marine $\delta^{13}C_{org}$ derived by photosynthetic pathways (*e.g.*, open marine plankton). However, the $\delta^{13}C_{org}$ record in nearshore facies can incorporate a number of locally controlled signals (Hayes, personal communication), and significant local stratigraphic variations in $\delta^{13}C_{org}$ are not uncommon. We report the ε_{TOC} index but consider it to be qualitative for shallow-water Tambien Group facies (Didikama Formation and Assem Limestone) due to the potential for early diagenetic modification of porewater $\delta^{13}C$.

6. Results

Table 1 reports petrographic sample descriptions and chemostratigraphic data for the four principal localities. We emphasize only least altered samples for $^{87}Sr/^{86}Sr$ and $\delta^{13}C_{carb}$ in the subsequent discussion, but for completeness all data are reported and shown in respective stratigraphic summary logs for each locality in Fig. 6A–D. The horizontal scale and order of geochemical parameters are identical in all plots to facilitate comparisons among localities, but the vertical stratigraphic thickness scale varies considerably. The following discussion is a condensed summary of significant litho- and chemostratigraphic findings. For the sake of space, detailed documentation of field relationships, lithostratigraphic and petrographic observations (with color photographs, Figs. S1–S7), general water depth facies interpretations, and related assessments of sample preservation are made available as supplementary online information (summarized in Table 2). It was useful to consider sample preservation on a systematic basis for each lithostratigraphic unit by comparing principal isotopic ($^{87}Sr/^{86}Sr$, $\delta^{18}O$, $\delta^{13}C$) and elemental (Sr, Fe, Mn) proxies, in addition to ASC. These variables were plotted using a multi-crossplot matrix for each carbonate lithostratigraphic interval; see supplementary materials (Bauerman, 1885; Folk, 1987; James et al., 1998; Kitachew, 1974Figs. S8–S15).

Table 2
Summary of supplemental online material.

S1. Detailed description of Tambien Group study localities	Figures	X-plot
A. Shiraro area		
A1. Didikama Formation	S1	S8
B. Mai Kenetal synclinorium		
B1. Werii Slate	S2	
B2. Assem Limestone	S3	S9
B3. Tsedia Slate (Logmiti Slate)		S10
B4. Mai Kenetal Limestone (Bilato Limestone and Slate and Tselim Imni Limestone)		S11
C. Negash Synclinorium		
C1. Madahne Alem, Lower Slate and Lower Didikama Formation	S4	S12
C2. Transect A–A′, Lower Didikama Formation, Negash Granite	S5	S13
C3. Transect B-B′, Didikama Formation		–
C4. Transect B–B′, Matheos Formation		
C4.1. Black Limestone and Transitional Members	S6	S14
C4.2. Diamictite Member		–
D. Samre area		
D1. Upper Tsaliet and Lower Tambien Groups	S7	S15
S2. Multi-crossplot matrices for assement of carbonate sample preservation		Figs. S8–S15 compiled by lithostratigraphic unit as indicated above

Note: Text references to supplement figures have an "S" prefix.

7. Discussion

7.1. Chemostratigraphic trends and regional correlation: synthesis

Fig. 7 presents study-wide chemostratigraphic results for samples considered least altered for $\delta^{13}C_{carb}$ and $^{87}Sr/^{86}Sr$, from which we infer regional correlation of the Tambien Group within Tigre. Here, we discuss the integration of separate transect results (detailed in the online supplement) into a coherent regional correlation scheme for the Tambien Group (Fig. 8). Recognition of negative $\delta^{13}C_{carb}$ intervals [grey-shaded fields in Fig. 7 (vertical) and Fig. 8 (horizontal)] constitutes an important starting point for correlations. We show that the succession of $\delta^{13}C_{carb}$ excursions, teamed with $^{87}Sr/^{86}Sr$ and Sr concentrations, establish an effective and internally consistent means for enhancing lithostratigraphic correlations among the investigated localities. Interpreted trends for these key indices are shown as dashed curves in Fig. 7. These relationships facilitate a composite chemostratigraphic reference section for the Tambien Group, which is introduced in Fig. 9. Age considerations, compositing basis, global correlations, and significance of chemostratigraphic trends are further examined in the companion manuscript (Miller et al., in prep.), but we suggest that the Tambien Group carbonate succession likely represents pre-"Sturtian" accumulation some time between *ca.* 775 and ~715–685 Ma. Optimal sample preservation exists within calcitic sections, especially those with consistently high Sr concentrations. The Mai Kenetal Limestone and Matheos Formation (Black Limestone member) are best preserved in terms of conventional indices for diagenetic screening. Dolomitic carbonates of the Didikama Formation are more variable, but show similar litho- and chemostratigraphic trends among Negash, Madahne Alem and Samre localities. Although these consistencies could repre-

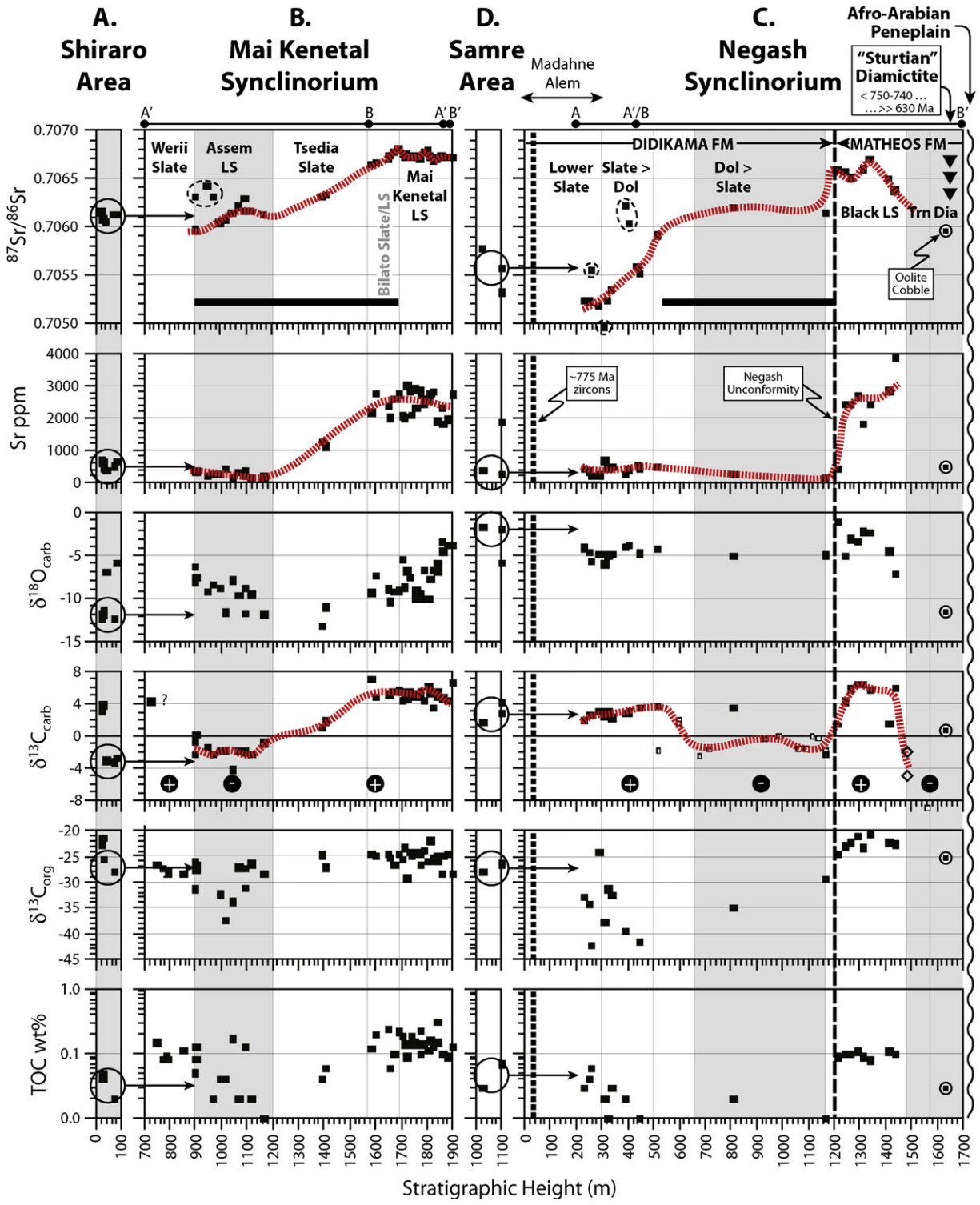

Fig. 7. Suggested chemostratigraphic correlations among Tambien Group transects for least-altered samples (Table 1). Dashed curves are suggested trends for seawater proxies most amenable for regional and global correlation. Outliers from the dominant $^{87}Sr/^{86}Sr$ trend (enclosed within dashed ellipses) are likely altered (see text). Grey-filled intervals denote strata with negative $\delta^{13}C_{carb}$ compositions. Open symbols in the Negash $\delta^{13}C_{carb}$ profile are from equivalent exposures in the eastern synclinorial limb (squares) and published data (diamonds) in Miller et al., 2003. The lower negative $\delta^{13}C_{carb}$ interval in Negash synclinorium begins several hundred meters above slates bearing ~775 Ma zircons (short-dashed line in C), interpreted as detrital. The Matheos Formation diamictite is constrained by detrital zircons to be younger than 750–740 Ma and by structural relations to be older than undeformed post-orogenic 'Mareb' granitoids (at least ~630 Ma in N. Ethiopia and Eritrea). Black horizontal bars in Mai Kenetal and Negash sequences show intervals interpreted as bounded by equivalent ages. The interval comparable to the Tsedia Slate (Mai Kenetal synclinorium) is interpreted as missing or highly condensed between the Didikama and Matheos Formation in Negash synclinorium (vertical long-dashed line).

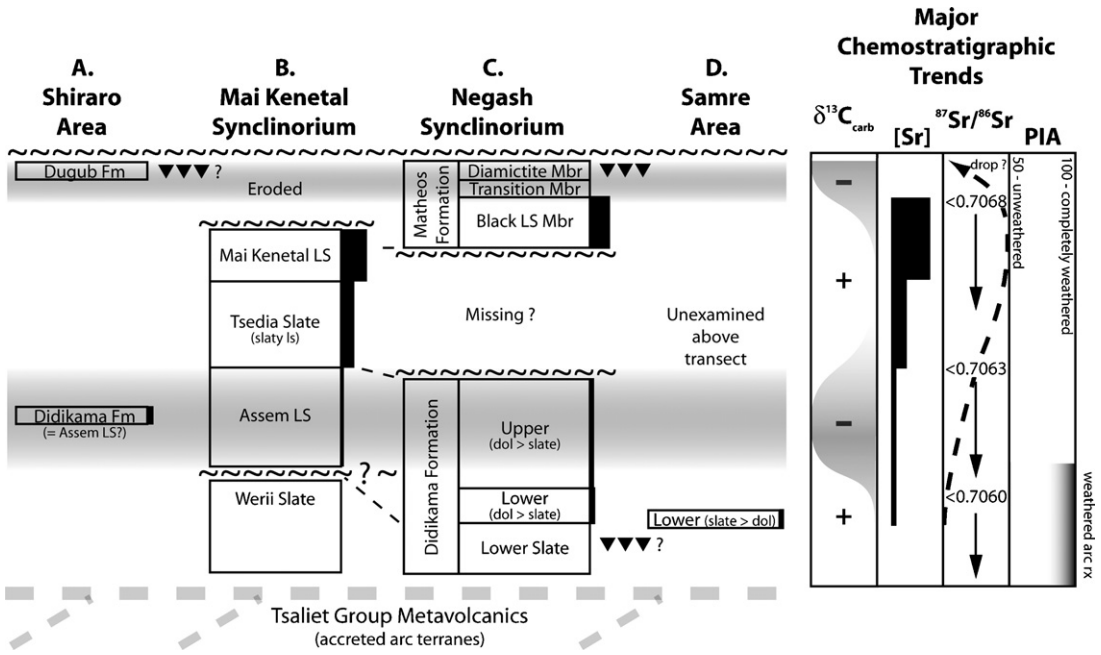

Fig. 8. Schematic regional stratigraphic framework for the Tambien Group based on lithostratigraphy and major chemostratigraphic trends. A crossover datum corresponding to the change from negative to positive $\delta^{13}C_{carb}$ values (with $^{87}Sr/^{86}Sr$ near 0.7063) and markedly higher (>1000 ppm) Sr concentrations is used to relate Mai Kenetal and Negash synclinoria.

sent primary depositional signatures, the extent to which Didikama dolomites retain primary open marine versus restricted marine compositions is unresolved.

In southern Tigre, least-altered Samre area samples appear to correlate within the lower (positive $\delta^{13}C_{carb}$) portion of the Didikama Formation in Negash (Fig. 7C–D), as further supported by lithologic character (slates with overlying intermittent dolomite beds, occurrence of prismatic cements, Fig. S7) and stratal position above the Tsaliet Group metavolcanics. The possible existence of a black limestone unit higher in the Samre section (apparent as a dark ridge-forming unit in satellite imagery, Fig. 4D) suggests that the regional synclinorial structure may also contain younger Tambien Group units similar to the Negash sequence (*i.e.*, Matheos Formation).

In western Tigre, Shiraro carbonate ridge samples appear to correlate within the Assem Limestone of Mai Kenetal (Fig. 7A–B) based on the combination of comparable negative $\delta^{13}C_{carb}$ and $^{87}Sr/^{86}Sr = 0.7061$ and sedimentologic properties (*i.e.*, carbonate units with significant intraclastic content, Fig. S1). These consistencies suggest a syngenetic link between the Assem Limestone and the upper Didikama Formation.

The regional lithostratigraphic framework for the Tambien Group carbonate succession supports an overall increase in water depths. Moderate energy shallow intertidal or subtidal settings are interpreted for the Assem Limestone (with prominent domal and interdigitate stromatolites, coarse rip-ups, and cross-bedded grainstones, Figs. S2–3) and a high alkalinity evaporitic tidal flat and intertidal setting for the lower Didikama Formation (evaporite pseudomorphs, microbial dololaminates, stromatolites, Fig. S5). Both of these lower carbonate units uniquely contain well-developed stromatolites and microbialites with sheet-crack cements, and have low TOC contents with highly variable $\delta^{13}C_{org}$—including light compositions consistent with nearshore environments (Fig. 7B and C, 9). Deeper subtidal environments with lower (but still variable) energy levels and ubiquitous micrite are interpreted for upper carbonate units of the Tambien Group, namely the Mai Kenetal Limestone and Matheos Formation. Both units are distinctive black limestones, characterized by fine horizontal layering with high lateral continuity (Fig. S3, D–H; Fig. S6, A–C). The lack of stromatolites and high-energy sedimentary structures (coarsely graded beds, cross bedding) but occurrence of dark intraclastic intervals and intraformational slumping may indicate slope deposition below storm wave base. Lastly, upper carbonate units are relatively enriched in TOC that has less variable $\delta^{13}C_{org}$, consistent with more open marine environments (Fig. 7B and C).

The lithostratigraphic relationship of Tambien Group units between Mai Kenetal and Negash synclinoria has remained enigmatic since they were proposed to be equivalent facies (Beyth, 1972). Subsequent interpretations suggested that the entire Negash sequence (Didikama + Matheos Formations) was younger than the Mai Kenetal sequence (Hailu, unpublished Adi Arkay map; Garland, 1980). Our litho- and chemostratigraphic data are entirely consistent with the Mai Kenetal carbonate sequence being syngenetic within the Negash lithostratigraphic continuum (Fig. 8). These results bolster similar findings from more limited data sets (Miller et al., 2004a,b, 2006; Alene et al., 2006). Paramount for this interpretation is recognition that the massive-bedded Mai Kenetal (= *Tselim Imne*) and Matheos Formation black limestone units are geochemically and lithostratigraphically equivalent, and furnish a gross, but unambiguous, tie horizon. These units stand out among all other Tambien Group units for their enrichment in $\delta^{13}C_{carb}$, $^{87}Sr/^{86}Sr$, and Sr (Fig. 7). With this tie, stratigraphic variations in $\delta^{13}C_{carb}$ indicate that the composite Tambien Group carbonate sequence records two consecutive positive-to-negative $\delta^{13}C_{carb}$ excursions, the first one within the upper portion of the Didikama Formation and Assem Limestone, and the second one preserved only in the transition to diamictite deposition within the Negash structure (Figs. 7–9). The Tambien Group is also characterized by a distinct stratigraphic increase in Sr content, beginning after the older positive-to-negative $\delta^{13}C_{carb}$ excursion (Figs. 7–9). We discuss the correlations between the four Tambien Group sequences, emphasizing Mai Kenetal and Negash synclinoria, in stratigraphic order according to changes in $\delta^{13}C_{carb}$ polarity.

The oldest significant Tambien Group carbonate production began as intermittent dolomite beds, positively enriched in $\delta^{13}C$ (mainly 2–4‰), within the lower slate-dominated portion of the

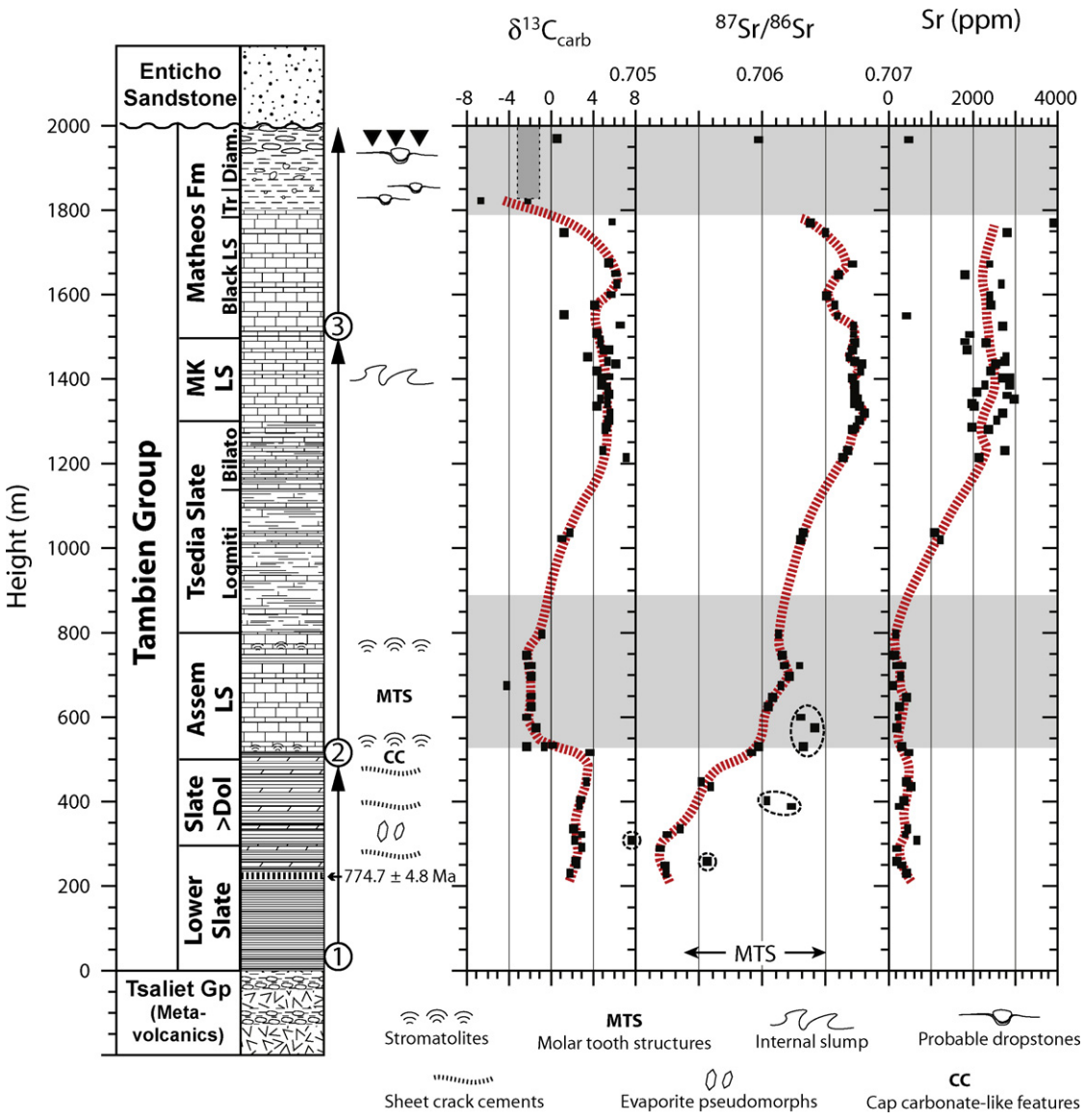

Fig. 9. Composite $\delta^{13}C_{carb}$, $^{87}Sr/^{86}Sr$, and [Sr] reference section for the Tambien Group. Dashed circles in $^{87}Sr/^{86}Sr$ plot denote samples interpreted as having altered compositions (*cf.* Fig. 7). The compositing basis (shown schematically in Fig. 8) is detailed in a companion manuscript. Arrowed stratigraphic segments 1 and 3 derive from Negash synclinorium. Segment 2 derives from Mai Kenetal synclinorium.

Didikama Formation in Negash (Madahne Alem, Transect A–A′) and Samre (Figs. 7D–C and 9). This interval is characterized by low TOC (med = 0.02 ± 0.02 wt.%) and Sr concentrations on the order of 300-400 ppm, with most (13/15) samples having $^{87}Sr/^{86}Sr$ less than 0.7059. The Samre $^{87}Sr/^{86}Sr$ data, although few and variable, are grossly consistent with the lower Didikama Formation in the Negash synclinorium, but fall well below the range determined for Shiraro and Mai Kenetal transects (Fig. 7A and B). The occurrence of microbialites/stromatolites, prismatic-isopachous cements and possible evaporite pseudomorphs (Figs. S5, S7), in addition to samples that are relatively enriched in $\delta^{18}O_{carb}$ (−4.2 ± 1.5‰) and highly depleted in $\delta^{13}C_{org}$ (med = −34.1 ± 5.7‰), suggests a shallow high-alkalinity/evaporative tidal flat setting with a significant contribution from chemosynthetic (methanogenic) bacteria.

We interpret the main lower Didikama Formation $^{87}Sr/^{86}Sr$ trend, from the better-sampled Negash transects, as a systematic rise from values between 0.7052 and 0.7059 (Figs. 7C and 9). Outliers from this trend are bimodal. Clearly altered carbonate with $^{87}Sr/^{86}Sr$ as low as 0.7048 (*i.e.*, T3-11-5) that is close to that measured within the Tsaliet metavolcanic succession at Samre (0.7047; T3-30-3), support the idea that porewater exchange with ensimatic materials could lower $^{87}Sr/^{86}Sr$ of altered carbonates. At the other extreme are two massive, coarsely recrystallized dolomitic marbles sampled near the Negash A–A′ granitoid (dashed circle in Fig. 7C), with $^{87}Sr/^{86}Sr$ (>0.7060), significantly more radiogenic than bounding transect samples (having better primary fabric retention). These samples may be altered by metasomatism associated with the 'Mareb' intrusion. The interpreted least-altered $^{87}Sr/^{86}Sr$ compositional range (0.7052–0.7059), although fairly unradiogenic, is not unprecedented in Neoproterozoic carbonate (*i.e.*, Asmerom et al., 1991; Kuznetsov et al., 1997; Kuznetsov, 1998 – in Melezhik et al., 2001); and thus could record a primary marine $^{87}Sr/^{86}Sr$ trend. The less parsimonious alternative is that lower Didikama dolomites were substantially altered to less radiogenic compositions due to the diagenetic influence of weathered Tsaliet Group metavolcanic constituents, and therefore the most radiogenic samples best approximate marine signatures. Either interpretation indicates a diminishing upsection influence in primary (seafloor hydrothermal) or secondary (diagenetic) ensimatic input.

On the basis of lithostratigraphic position above the Tsaliet Group metavolcanics, we infer that the Werii Slate in Mai Kenetal synclinorium correlates with or below the lower Didikama Formation at Negash (Figs. 7 and 8), possibly equivalent to the lower slate member (Fig. 3C; this study), and was deposited when seawater had positive $\delta^{13}C_{DIC}$. The only Werii Slate carbonate $\delta^{13}C_{carb}$ analysis (+4.3‰) is from fine dolomite laminae within a varve-like slate interval (Fig. S2C) near the top of the unit. The extent to which this sample reflects a primary marine composition is uncertain, but its positive composition is similar to the lower Didikama Formation (Fig. 7). Werii Slate TOC (med = 0.08 ± 0.08 wt%) and $\delta^{13}C_{org}$ (med = −27.2 ± 1.6‰) are slightly enriched compared to basal Didikama sequences in Negash synclinorium but comparable to those in Samre (TOC avg: 0.06 ± 0.03wt%; $\delta^{13}C_{org}$ avg: −26.4 ± 1.6‰). Modeling of the temporal C-isotopic fractionation between TOC and carbonate (Hayes et al., 1999: Fig. 1) suggests that >750 Ma seawater had positive $\delta^{13}C_{DIC}$, the timing of which is compatible with Werii Slate deposition. The Werii Slate bulk and trace element composition suggests deposition in association with a well-developed island arc system (Sifeta et al., 2005). The predominance of fine-grained detritus and high chemical weathering indices suggest a deeply weathered source area. The finely laminated appearance and $\delta^{13}C_{org}$ composition near the top of the Mai-Kenetal Werii sequence (Fig. S2, B–D; Fig. 7) further indicate a quiet water depocenter that primarily preserved photosynthetic (primary phytoplankton producer) biomass.

The lack of lower carbonate units with positive $\delta^{13}C$ and $^{87}Sr/^{86}Sr < 0.7059$ in Mai Kenetal synclinorium (Fig. 7B) could manifest a cryptic disconformity at the Werii Slate-Assem Limestone contact, the gap being equivalent to the lower Didikama (slate>dol) Formation at Negash (Fig. 8). Chemical weathering indices for the Werii Slate and lower Didikama Formation (lower slate and slate>dol members) are similar (PIA: 92-99, Table 1, Fig. 8) and support intense silicate weathering of the Tsaliet arc accretion complex during a time when marine $\delta^{13}C_{DIC}$ was positive. Moderate to extreme weathering (PIA >75, $n = 24$) is also indicated for the Werii Slate east of Mai Kenetal (Fig. 2; see Sifeta et al., 2005). The considerable thickness of lower Tambien Group slate (~1.1 km Werii Slate, ≥0.5 km lower Didikama Fm; Beyth, 1972) with aggressive silicate weathering indices, suggest that warm humid climates (Nesbitt and Young, 1982) prevailed over a lengthy depositional interval prior to significant carbonate accumulation in the Tambien Group.

Tambien Group $\delta^{13}C_{carb}$ polarity next shifts to negative compositions in the upper dolomite-dominated portion of the Didikama Formation (Negash) and Assem Limestone (Mai Kenetal). Negative $\delta^{13}C_{carb}$ compositions for upper Didikama dolomites (med = −1.7 ± 0.8‰; $n = 10$) compare well with least altered Assem Limestone values (med = −1.7 ± 1.1‰; $n = 13$), as do Sr concentrations (250 ± 80 ppm), despite their contrasting mineralogies. Stromatolitic facies were recognized in both sequences, but more stringent sedimentologic comparisons are limited by poorer exposures and loss of primary depositional fabrics associated with upper Didikama dolomite (Negash). Accordingly, most of the insights to Tambien Group deposition during this negative $\delta^{13}C_{carb}$ interval are derived from the Assem Limestone in Mai Kenetal synclinorium.

The change to negative $\delta^{13}C_{carb}$ appears to begin at or above $^{87}Sr/^{86}Sr = 0.7059$ and stratigraphically highest values for the negative $\delta^{13}C_{carb}$ interval are 0.7061–0.7062 in both sequences. The strontium isotopic composition of Assem Limestone samples varies considerably between 0.7059 and 0.7064. Although the curve may possess more structure, we draw the curve as a lower running limit (Figs. 7B and 9) because of the similarity in $^{87}Sr/^{87}Sr$ determined for the upper Didikama Formation and evidence from the basal Assem Limestone for more radiogenic carbonate compositions (probably from late ferroan calcite cement) in immediate proximity to slate intervals (e.g., Fig. S2E). We consider the dominant $^{87}Sr/^{87}Sr$ trend to be a continuation of the lower Didikama rise, but at a decreasing (stratigraphic) rate (Figs. 7B and 9).

The Assem Limestone was deposited in a variably energetic intertidal or subtidal setting, above fair weather base, beginning abruptly above the Werii Slate. Its highly variable TOC and $\delta^{13}C_{org}$ suggest the interplay of shallow marine environments dominated by biomass produced via primary photosynthetic as well as methanogenic pathways. The basal contact constitutes a significant change in depositional style and the basal dolomite bed of the Assem Limestone shares many sedimentological and isotopic characteristics of cap carbonates [*i.e.*, abrupt basal lithologic transition to high energy carbonate facies, basal dolomite transitioning upward into limestone, consistently negative $\delta^{13}C_{carb}$, primary and/or early diagenetic (pre-compaction) prismatic and radial fibrous cements (Fig. S2D–G; cf. Kennedy et al., 2001) that appear to have formed near the sediment-water interface (implying critically oversaturated seawater and/or pore fluids, i.e., Hoffman et al., 2007)]. A potential cap carbonate raises the possibility of an underlying glacial association (either within the upper Werii Slate or at its contact with the Assem Limestone - as a glacial unconformity) or that there are non-glacigenic cap carbonates. Although the Werii Slate-Assem Limestone contact is well exposed and appears conformable, the diverse lithologic associations suggest that this may be an unconformity/sequence boundary. A similarly abrupt contact was not delineated within the Negash sequence, although the top of the Didikama Formation lower slate member in the eastern synclinorial limb contains a possible glacigenic interval (Beyth et al., 2003; volcanic conglomerates and greywackes below spotted slate) that could correlate to the upper Werii Slate. The lower negative $\delta^{13}C_{carb}$ interval in dolomites of the upper Didikama Formation initiates several hundred meters higher than a felsic slate interval bearing ~775 Ma zircons (Madahne Alem locality: Fig. 7C and 9; Supplement C1, Fig. S12). This suggests that any glacial association should be younger than ~775 Ma and older than the capping diamictite of putative "Sturtian" affiliation [younger than 750–740 Ma (youngest diamictite zircons, Avigad et al., 2007) and older than 630 Ma (oldest Tigrean post-orogenic 'Mareb' granitoids)]. These constraints implicate a possible association with the ~755 Ma Kaigas glaciation (Hoffmann et al., 2006).

The next $\delta^{13}C_{carb}$ shift toward positive compositions begins in the Mai Kenetal synclinorium within the uppermost Assem Limestone (~−2‰) and $\delta^{13}C_{carb}$ rises throughout Tsedia Slate and Bilato Slate/Limestone deposition, culminating as a well-defined plateau (med: 5.3 ± 0.8‰) in the Mai Kenetal Limestone (Fig. 7B). Paralleling this rise are increases in $^{87}Sr/^{86}Sr$ and [Sr] and possibly also $\delta^{13}C_{org}$ and TOC (Figs. 7B and 9). The equivalent of the Tsedia Slate seems to be largely absent or highly condensed at Negash, as there appears to be an abrupt and extreme change in $\delta^{13}C_{carb}$, $^{87}Sr/^{86}Sr$, and [Sr] at, or near, the Didikama-Matheos Formation contact. This interface warrants further scrutiny as an unconformity in view of the juxtaposition of high [Sr] black limestones of the Matheos Formation directly on top of low [Sr] dolomites of the Didikama Formation. Although the contact was conformable in our transect areas, a slight angular unconformity occurs along this contact in the northern Negash synclinorium (Adigrat sheet, Garland, 1980). These observations suggest that a portion of the Negash Tambien Group sequence experienced relative uplift and was removed by erosion during Tambien time. Because of the limited sampling of the upper Tsedia slate sequence, a lesser unconformity is also possible within the Mai Kenetal Tambien sequence. We note however that this stratigraphic interval seems to involve a gradual lithologic transition without a major change in mineralogy. The Tsedia Slate is of particular importance for prospective Tambien Group correlations because in addition to dramatic (~7‰) enrichment in $\delta^{13}C_{carb}$, it apparently also involves the greatest stratigraphic rates of change in $^{87}Sr/^{86}Sr$, and [Sr] (Fig. 9). Tsedia Slate strontium isotope compositions

increase from 0.7062 to 0.7067, and there is an associated ninefold increase in Sr concentrations (med: 2465 ± 381 ppm) above levels in the Assem Limestone (med: 267 ± 166 ppm). Strontium isotope compositions reach a maximum of 0.7068 near the base of the Mai Kenetal Limestone, followed by a plateau of remarkably stable values (med = 0.706730 ± 35; n = 25) throughout the rest of the unit. In the Negash structure, the Matheos Formation Black Limestone has geochemical and isotopic properties nearly identical to the Mai Kenetal Limestone. Major differences are somewhat lower $^{87}Sr/^{86}Sr$ (med = 0.706574 ± 102) and higher $\delta^{13}C_{org}$ (−22.6 ± 1.2‰ vs. −24.9 ± 1.6‰ for the Mai Kenetal Limestone). Strontium isotope compositions for the Matheos Formation Black Limestone Member show minor systematic variations culminating in a maximum of 0.70671, and then fall to 0.70639 or lower in uppermost limestones approaching the Diamictite Member (Fig. 7). We suggest that Matheos Formation Black Limestone deposition began within the upper part of, or above, the Mai Kenetal Limestone. In support of this inference we note the comparable lithology (massive-bedded, homogeneous black limestone, finely layered in thin section) and similarity between $^{87}Sr/^{86}Sr$ and $\delta^{13}C_{org}$ between highest and lowest facies of the Mai Kenetal and Matheos Formation limestones, respectively (cf. Fig. 6B and C2). Also consistent with this correlation is a strong $\delta^{18}O$ enrichment trend in the upper Mai Kenetal Limestone that appears to continue in the lower 150 m of the Matheos Formation black limestone (Fig. 7B and C).

The final segment of Tambien Group depositional history involves a return to negative $\delta^{13}C_{carb}$, preserved only within the transition from Matheos Formation black limestone to diamictite deposition (Figs. 7C and 9). This transition (see supplement) involves thinning and disappearance of limestone beds (some with $\delta^{13}C_{carb}$ as low as −6.5‰, Miller et al., 2003) with increasing intercalation of non-calcareous slate prior to the appearance of polymictic clasts (Fig. S6C-I). Matrix carbonate in nine Negash diamictite samples (Fig. 7C) has average $\delta^{13}C_{carb}$ of −2.0 ± 1.0‰ and $\delta^{18}O_{carb}$ of −7.5 ± 1.7‰ (Miller et al., 2003). Although their primary origin is uncertain, the lack of positive $\delta^{13}C_{carb}$ typical of the lower Matheos Formation black limestone seems most compatible with a marine transition to negative $\delta^{13}C_{DIC}$. The alternatives are that diamictite matrix carbonate is principally detrital, arising from erosion of an earlier negative $\delta^{13}C$ carbonate unit, and/or formed diagenetically within porewaters that were highly depleted in $\delta^{13}C$ relative to ambient seawater. The apparent trend of decreasing $^{87}Sr/^{86}Sr$ in uppermost Matheos black limestones approaching diamictite deposition could reflect diagenetic alteration in conjunction with chemical weathering of glacially unroofed Tsaliet highlands or a secular change in seawater to less radiogenic values, perhaps reflecting pronounced dampening of riverine continental Sr runoff and concomitant enrichment in oceanic hydrothermal Sr due to ice cover.

7.2. Tectonic and eustatic influences on Tambien Group lithostratigraphy

The general accreted arc tectonic setting of the southern ANS, with waning magmatic activity between ~780 and 740 Ma (see Avigad et al., 2007), in addition to chemo- and lithostratigraphic evidence for a Didikama-Matheos Formation unconformity (high Sr limestone directly overlying low Sr dolomite, angular unconformity in N. Negash), suggest that a combination of tectonism and eustasy may have influenced regional physiography within the greater Tambien/Mozambique basin during deposition of the lower Tambien Group. Relative uplift in the Negash depocenter, prior to Matheos Formation limestone deposition, may have unroofed a considerable portion (~Tsedia Slate equivalent; dolomitic?) of the Tambien Group record, whereas comparable uplift and erosion was not recorded in the Mai Kenetal depocenter. The similarity of geochemical characteristics observed in stratigraphically higher and probable deeper water Mai Kenetal and Matheos Black limestones argues that they are broadly correlative. The blanket-like nature of these units above more variable lower Tambien Group units in Tigre (Mai Kenetal, Negash, and possibly Samre) may reflect diminished relief, perhaps aided by relative sea level rise (and/or regional subsidence of the Mozambique basin within the southern ANS).

Although prospective older Cryogenian sequences have been identified in the ANS (Stern et al., 2006), the geographic distribution of "Sturtian" glaciation(s) is unknown. Peneplanation of the Neoproterozoic sedimentary record throughout the Afro-Arabian region (Avigad et al., 2005) is clearly a significant preservational limitation to any such evaluation. The Matheos Formation (Negash) diamictite and Shiraro Group siliciclastics (Avigad et al., 2007) are the only prospective "Sturtian" glaciogenic units yet identified in Tigre. Occurrence of molar tooth structure (Assem Limestone, Fig. S3C) and lack of any Tambien carbonate $^{87}Sr/^{86}Sr > 0.7068$ below the Matheos diamictite (Figs. 7 and 8) support its "Sturtian" glacial affiliation, and virtually exclude a Marinoan context (see Shields, 2002; Fairchild and Kennedy, 2007). The demonstrably marine pre-"Sturtian" chemostratigraphic pretext for the Matheos diamictite corroborates lithostratigraphic arguments that it is Tigre's youngest preserved Cryogenian glacial deposit. Although diamictite clast compositions could have a local stratigraphic origin, the only firm control on proximity derives from detrital zircon ages (Avigad et al., 2007). The distribution of these ages (~0.85–0.74 Ga, plus a minor fraction of likely inherited 1.1 Ga zircons) broadly reflects origins from ANS basement (Avigad et al., 2007), thus diamictite could equally originate over a large area many hundreds of kilometers in extent. Active tectonism during lower Tambien Group deposition could be significant for later generation of "Sturtian" diamictites because glacial scouring of regional physiographic highs (areas of prior Tambien uplift and/or unroofing) during the "Sturtian" glacioeustatic lowstand could readily provide subsequent glacial diamictites with clasts representative of earlier Tsaliet-Tambien deposition. This scenario adds to hypotheses accounting for "Sturtian" diamictite genesis, but reiterates the importance of "relief differentiation in shaping the glacial record of the southern ANS" (Avigad et al., 2007).

7.3. Do Tambien Group chemostratigraphic profiles record global secular variations in early Cryogenian ocean chemistry?

Verifying global Neoproterozoic isotope signals is challenged by: (1) sample preservation, which is difficult to establish; (2) stratigraphic resolution sufficient to characterize the stratigraphic rate and magnitude of secular variations; and (3) radiometric age constraints sufficiently narrow to provide unambiguous correlations with other records. Accurate interpretation of Neoproterozoic isotope stratigraphy also requires improved understanding of the origin (abiotic vs. biotic) of carbonate used to establish isotope stratigraphies, specifically, whether open marine compositions are recorded and preserved in carbonate produced abiotically and/or in association with microbes.

Tambien Group carbonates are mainly low greenschist, neomorphosed (microspar and dolomicrospar), primary and resedimented microbialaminite units, presumably formed from fine carbonate mud (micrite) precipitated at or near the sediment-water interface in association with relatively well-mixed and isotopically homogeneous shallow surface waters of the Mozambique Ocean. Lithologies include dolomite and limestone, with limestones showing a stratigraphic increase in [Sr] to levels suggestive of primary aragonitic compositions. Dolomites preserve indications of evaporites and isopachous crusts (see supplement), possibly indicating primary or early authigenic marine (abiotic?) cements. Tambien Group marine ecosystems were likely dominated by a

host of autotrophic and heterotrophic bacteria and non-calcareous algae/acritarchs. These biotic constituents obviously contrast with skeletal carbonates used to refine the record of Phanerozoic seawater variation, not only in terms of how associated carbonate mineralized, but also in terms of our ability to systematically sample discrete carbonate phases and evaluate preservation.

Precambrian carbonates have long been regarded as primary precipitates from supersaturated seawater that record ambient physicochemical and biological conditions. However, modern oceans have significant kinetic inhibitors for direct precipitation of calcium carbonate or dolomite (*e.g.*, ion-complexing, cation hydration, and pH-dependent carbonate ion concentration/activity). Wright and Oren (2005) summarize mounting evidence that microbial activities can overcome these kinetic inhibitors by influencing microscale solution chemistry (namely, by increasing pH and concentrations of Ca^{2+}, Mg^{2+}, and CO_3^{2-} ions beyond saturation). In particular, they suggest that heterotrophic non-photosynthetic bacteria (aerobic and anaerobic) may have catalyzed large-scale carbonate precipitation (bacterial carbonatogenesis) prior to the evolution of skeletal calcifying organisms. The possibility that Cryogenian carbonate production was substantially microbial has significant implications for interpreting the origin of micrite/dolomicrite and associated microspar/dolomicrospar fabrics.

The significant question for isotope chemostratigraphy is to what extent do microbial carbonates mirror primary seawater isotopic compositions and record long-term secular variations? Microbial micrite production likely involved interacting metabolic ecologies (*i.e.*, phototrophs, chemoautotrophs, chemoheterotrophs). Water chemistry, for example oxygen content and by association nitrate and sulfate could have impacted the importance of microbial communities and the locus of carbonatogenesis relative to the sediment-water interface. This would control both the amount of organic carbon-fixed as carbonate, and the isotopic composition of carbonate. Over what regional scale could such processes have operated? Because of the possibility that Cryogenian carbonates were significant products of bacterially influenced ecosystems, not necessarily in equilibrium with open marine seawater $\delta^{13}C_{DIC}$, $^{87}Sr/^{86}Sr$ (which is not similarly susceptible to biotic fractionations) may be more representative of primary oceanic compositions. Early authigenic or penecontemporaneous microbial carbonate might also have initial $\delta^{18}O$ compositions representative of ambient bottom waters (temperature/salinity/pH), but water-rock interaction is most likely to alter this isotopic system.

Although these variables remain poorly understood and deserve to be better studied, Neoproterozoic C-isotope stratigraphies appear to work (are reproducible in disparate outcrops) on at least local and regional scales (*e.g.*, Robb et al., 2004; Halverson et al., 2005; Hoffman et al., 2007), albeit with potential water mass facies variations. Globally correlative signals that track (directly or indirectly) intrinsic characteristics of seawater thus remain possible and the common observation of negative $\delta^{13}C$ excursions associated with transition to and from glacigenic deposits supports a global linkage between the carbon cycle and climatic transitions. The Tambien Group chemostratigraphic framework adds empirical support that integrating $^{87}Sr/^{86}Sr$ with $\delta^{13}C$ provides an even more effective correlation tool for the Neoproterozoic. Refining the "integrated" isotope correlation tool and verifying its global application will require comparative studies of similarly integrated data sets from time-equivalent marine units.

8. Conclusions

The Tambien Group of northern Ethiopia (Tigre) represents an intra-oceanic (arc-accretion carbonate platform) setting that records the early Neoproterozoic evolution of the Mozambique Ocean realm of the ANS. The Tambien Group carbonate succession preserves a regionally coherent pre-"Sturtian" sedimentary record that followed the demise of arc-magmatism in the southern ANS (*c.* 775–740 Ma). Its capping "Sturtian" glacial diamictite (Negash – Matheos Formation) is not yet precisely dated but was deposited well before intensive orogenic compression and subsequent *c.* 630–610 Ma post-orogenic magmatism, respectively associated with incipient and mature development of the EAO. The regional lithostratigraphic and chemostratigraphic record of the Tambien Group seems to be internally consistent for $\delta^{13}C_{carb}$, $^{87}Sr/^{86}Sr$, and [Sr], enabling widespread correlation between virtually unknown (Shiraro area and Samre area carbonate) and better-studied (Mai Kenetal and Negash) outcrops. $\delta^{18}O_{carb}$ is more variable, but there are also gross regional stratigraphic consistencies that could reflect secular marine variation in the lead up to "Sturtian" glaciation. Negash synclinorium spans the carbonate depositional histories of all other localities but may contain a significant unconformity, suggesting at least local structural relief differentiation during deposition of the early Tambien Group carbonate platform. On the basis of regional consistency and intersection with the range of pre-"Sturtian" $^{87}Sr/^{86}Sr$ (*e.g.*, Melezhik et al., 2001), lower Tambien Group (Didikama Formation) dolomites with moderate Sr concentrations (*e.g.*, 250–500 ppm) and good retention of primary depositional textures appear to largely retain depositional $^{87}Sr/^{86}Sr$ compositions.

The baseline Tambien Group record involves two consecutive positive-to-negative $\delta^{13}C_{carb}$ excursions on a backdrop of increasing $^{87}Sr/^{86}Sr$ and [Sr] (Figs. 8 and 9). The first negative excursion likely occurred during waning arc-magmatism in the southern ANS (*c.* 780–740 Ma), with least altered $^{87}Sr/^{86}Sr$ compositions no lower than 0.7059. Occurrence of cap carbonate-like features at the base of this excursion (Assem Limestone), prospective glacigenic intervals regionally at lower stratigraphic intervals, and severe silicate weathering indices associated throughout the underlying 1.1 km Werii Slate (Mai Kenetal synclinorium) and $\geq$0.5 km Lower Slate of the Didikama Formation (Negash and Samre) may record the influence of an earlier pre-"Sturtian" cooling event, perhaps related to the *c.* 755 Ma Kaigas glaciation (Hoffmann et al., 2006). If so, the Assem Limestone is the first cap carbonate sequence recognized in the ANS. The second negative $\delta^{13}C_{carb}$ excursion occurs in the stratigraphic transition to "Sturtian" glacial diamictite, following a stratigraphic plateau in $\delta^{13}C$ (5.3–5.7‰) and $^{87}Sr/^{86}Sr$ (0.7066–0.7068). The Tambien group sequence between the two negative $\delta^{13}C$ excursions is characterized by increasing $\delta^{13}C$ and $^{87}Sr/^{86}Sr$ and [Sr] (Fig. 9), which should offer improved Neoproterozoic correlation potential – if verified in other pre-"Sturtian" marine carbonate settings.

Acknowledgements

This study was supported by US-Israel Binational Science Foundation grant 2002337. We thank Kiros Mehari, Dirk Küster, and Tarekegn Tadesse for field expertise and assistance, and logistical support from Mekele University during field seasons. We thank Amenti Abraham, Chief Geologist, Geological Survey of Ethiopia, who encouraged and supported our study, and Avner Ayalon, Geological Survey of Israel, for his contribution to stable isotopic analyses. Dean Tuck prepared slate samples and contributed to the assessment of weathering indices. James Talbot (K/T Geoservices, Inc.) provided supporting XRD analyses. We are grateful to Todd Housh and Jay Banner (Univ. of Texas at Austin) for providing access to dynamic mode $^{87}Sr/^{86}Sr$ measurement by TIMS. Thanks are also due to thoughtful reviews by Graham Shields and Mike

Pope, which strengthened the manuscript. Lastly, we would like to acknowledge numerous thought-provoking discussions arising from participation in IGCP project 512 'Neoproterozoic Ice Ages' (www.IGCP512.com <http://www.igcp512.com/>).

Appendix A. Supplementary data

Supplementary data associated with this article can be found, in the online version, at doi:10.1016/j.precamres.2008.12.004.

References

Alene, M., Conti, A., Sacchi, R., Zuppi, G., 1999. Stable isotope composition (13C and 18O) of Neoproterozoic limestones and dolomites from Tigre, North Ethiopia. Bollettino della Società Geologica Italiana 118, 611–615.

Alene, M., Jenkin, G.R.T., Leng, M.J., Darbyshire, D.P.F., The Tambien Group, 2006. Ethiopia: an early Cryogenian (ca. 800–735 Ma) neoproterozoic sequence in the Arabian–Nubian shield. Precambrian Research 149, 79–89.

Anbar, A.D., Knoll, A.H., 2002. Proterozoic ocean chemistry and evolution: a bioinorganic bridge? Science 297, 1137–1142.

Arkin, Y., Beyth, M., Dow, D.B., Levitte, D., Haile, T., Hailu, T., 1971. Geological map of Mekele Sheet area ND37-11 Tigre Province. Imperial Ethiopian Government, Ministry of Mines. Geological Survey of Ethiopia. Scale 1, 250,000.

Asmerom, Y., Jacobsen, S.B., Knoll, A.H., Butterfield, N.J., Swett, K., 1991. Strontium isotopic variations of Neoproterozoic seawater: implications for crustal evolution. Geochimica et Cosmochimica Acta 55, 2883–2894.

Asrat, A., Barbey, P., Ludden, J.N., Reisberg, L., Gleizes, G., Ayalew, D., 2004. Petrology and isotope geochemistry of the Pan-African Negash Pluton, northern Ethiopia; mafic-felsic magma interactions during the construction of shallow-level calcalkaline plutons. Journal of Petrology 45, 1147–1179.

Avigad, D., Sandler, A., Kolodner, K., Stern, R.J., McWilliams, M.O., Miller, N., Beyth, M., 2005. Mass-production of Cambrian quartz-rich sandstone as a consequence of chemical weathering of Pan-African orogens: implications for global environment. Earth and Planetary Science Letters 240, 818–826.

Avigad, D., Stern, R.J., Beyth, M., Miller, N., McWilliams, M., 2007. Detrital zircon U–Pb geochronology of Cryogenian diamictites and lower Paleozoic sandstone in Ethiopia (Tigrai): age constraints on Neoproterozoic glaciation and crustal evolution of the southern Arabian–Nubian Shield. Precambrian Research 154, 88–106.

Baker, P.A., 1990. Strontium isotopic stratigraphy utilizing authigenic dolomites in hemipelagic sediments (abstract). American Association of Petroleum Geologists Bulletin 74, 604.

Banner, J.L., Hanson, G.N., 1990. Calculations of simultaneous isotopic and trace element variations during water–rock interaction with applications to carbonate diagenesis. Geochimica et Cosmochimica Acta 54, 3123–3137.

Bauerman, H., 1885. Report on the geology of the country near the forty-ninth parallel of north latitude west of the Rocky Mountains. Geological Survey of Canada, Report of Progress 1882–1884, Pt. B, 1–42.

Beeunas, M.A., Knauth, L.P., 1985. Preserved stable isotopic signature of subaerial diagenesis in the 1.2-B.Y.Mescal Limestone, Central Arizona: implications for the timing and development of a terrestrial plant cover. Geological Society of America Bulletin 96, 737–745.

Bernoulli, D., Gasperina, L., Bonatti, E., Stille, P., 2004. Dolomite formation in pelagic limestone and dolomite, Romanche Fracture Zone, equatorial atlantic. Journal of Sedimentary Research 74, 924–932.

Beyth, M., 1971. A suggestion for interpretation of the stratigraphy of northern Ethiopia according to the model of plate tectonics. Geology 1, 81–82.

Beyth, M., 1972. The geology of central western Tigre, Ethiopia Ph.D. Thesis. Bonn, University of Bonn, 155 p.

Beyth, M., Avigad, D., Wetzel, H.U., Matthews, A., Berhe, S.M., 2003. Crustal exhumation and indications for Snowball Earth in the East African Orogen: North Ethiopia and East Eritrea. Precambrian Research 123, 187–201.

Bowring, S.A., Grotzinger, J.P., Condon, D.J., Ramezani, J., Newall, M., 2007. Geochronologic constraints on the chronostratigraphic framework of the Neoproterozoic Huqf Supergroup. Sultanate of Oman. American Journal of Science 307, 1097–1145.

Brand, U., Veizer, J., 1980. Chemical diagenesis of a multicomponent carbonate system: 1. Trace elements. Journal of Sedimentary Petrology 50, 1219–1236.

Burdett, J.W., Grotzinger, J.P., Arthur, M.A., 1990. Did major changes in the stable-isotope composition of Proterozoic seawater occur? Geology 18, 227–230.

Burns, S.J., Baker, P.A., 1987. A geochemical study of dolomite in the Monterey Formation, California. Journal of Sedimentary Petrology 57, 128–139.

Burns, S.J., Baker, P.A., Showers, W.J., 1988. The factors controlling the formation and chemistry of dolomite in organic-rich sediments: Miocene Drakes Bay Formation, California. Sedimentology and Geochemistry of Dolostones. SEPM Special Publication, vol. 43, pp. 41–52.

Canfield, D.E., Raiswell, R., 1999. The evolution of the sulfur cycle. American Journal of Science 299, 697–723.

Canfield, D.E., Teske, A., 1996. Late Proterozoic rise in atmospheric oxygen concentration inferred from phylogenetic and sulphur-isotope studies. Nature 382, 127–132.

Canfield, D.E., Poulton, S.W., Narbonne, G.M., 2007. Late-neoproterozoic deep-ocean oxygenation and the rise of animal life. Science 315, 92–95.

Coplen, T.B., 1988. Normalization of oxygen and hydrogen isotope data. Chemical Geology (Isotope Geoscience Section) 72, 293–297.

Craig, H., 1957. Isotopic standards for carbon and oxygen and correction factors for mass-spectrometric analysis of carbon dioxide. Geochimica et Cosmochimica Acta 12, 133–149.

De Souza Filho, C.R., Drury, S.A., 1998. A Neoproterozoic supra-subduction terrane in northern Eritrea, NE Africa. Journal of the Geological Society, London 155, 551–566.

Derry, L.A., Keto, L.S., Jacobsen, S.B., Knoll, A.H., Swett, K., 1989. Sr isotopic variations in upper Proterozoic carbonates from Svalbard and East Greenland. Geochimica et Cosmochimica Acta 53, 2331–2339.

Derry, L.A., Kaufman, A.J., Jacobsen, S.B., 1992. Sedimentary cycling and environment change in the late Proterozoic: evidence from stable and radiogenic isotopes. Geochimica et Cosmochimica Acta 56, 1317–1329.

DesMarais, D.J., Strauss, H., Summons, R.E., Hayes, J.M., 1992. Carbon isotope evidence for the stepwise oxidation of the Proterozoic environment. Nature 359, 605–609.

Drury, S.A., Berhe, S.M., 1993. Accretion tectonics in northern Eritrea revealed by remotely sensed imagery. Geological Magazine 130, 177–190.

Eyles, N., Januszczak, 2004. 'Zipper-rift': a tectonic model for Neoproterozoic glaciations during the breakup of Rodinia after 750 Ma. Earth Science Reviews 65, 1–73.

Fairchild, I.J., Kennedy, M.J., 2007. Neoproterozoic glaciation in the Earth System. Journal of the Geological Society, London (subject to corrections in proof).

Fairchild, I.J., Spiro, B., 1987. Petrological and isotopic implications of some contrasting Late Precambrian carbonates, NE Spitsbergen. Sedimentology 34, 973–989.

Fairchild, I.J., Marshall, J.D., Bertrand-Sarfati, J., 1990. Stratigraphic shifts in carbon isotopes from Proterozoic stromatolitic carbonates (Mauritania): influences of primary mineralogy and diagenesis. American Journal of Science 290A, 46–79.

Fairchild, I.J., Spiro, B., Herrington, P.M., Song, T., 2000. Controls on Sr and C isotope compositions of Neoproterozoic Sr-rich limestones of East Greenland and North China. In: Grotzinger, J.P., James, N.P. (Eds.), Carbonate Sedimentation in the Evolving Precambrian World, 67. SEPM Special Publication, pp. 297–313.

Fanning, C.M., 2006. Constraints on the timing of the Sturtian glaciation from southern Australia; *i.e.*, for the true Sturtian. Geological Society of America Abstracts with Programs 38, 115.

Fedo, C.M., Nesbitt, H.W., Young, G.M., 1995. Unraveling the effects of potassium metasomatism in sedimentary rocks and paleosols, with implication for paleoweathering conditions and provenance. Geology 23, 921–924.

Folk, R.L., 1987. Detection of organic-matter in thin-sections of carbonate rocks using a white card. Sedimentary Geology 54, 193–200.

Garland, C.R., 1980. Geology of the Adigrat area. Ministry of Mines Memoir No. 1, 51 p. Addis Ababa 1:250,000 map.

Halverson, G.P., 2006. A neoproterozoic chronology. In: Xiao, S., Kaufman, A.J. (Eds.), Neoproterozoic Geobiology and Paleobiology. Springer, Dordrecht, The Netherlands, pp. 231–271.

Halverson, G.P., Hoffman, P.F., Schrag, D.P., Maloof, A.C., Rice, A.H.N., 2005. Toward a neoproterozoic composite carbon-isotope record. Geological Society of America Bulletin 117, 1181–1207.

Halverson, G.P., Dudás, F.Ö., Maloof, A.C., Bowring, S.A., 2007. Evolution of the $^{87}Sr/^{86}Sr$ composition of Neoproterozoic seawater. Palaeogeography, Palaeoclimatology, Palaeoecology 256, 103–129.

Hayes, J.M., Strauss, H., Kaufman, A.J., 1999. The abundance of 13C in marine organic matter and isotopic fractionation in the global biogeochemical cycle of carbon during the past 800 Ma. Chemical Geology 161, 103–126.

Hoffman, P.F., 2004. Neoproterozoic snowball Earth; exercising the imaginative muscle. Geobulletin 47, p. 3, 5, 10–11, 13, 24–25, 33.

Hoffman, P.F., Schrag, D.P., 2002. The snowball earth hypothesis: testing the limits of global change. Terra Nova 14, 129–155.

Hoffman, P.F., Kaufman, A.J., Halverson, G.P., Schrag, D.P., 1998. A neoproterozoic snowball earth. Science 281, 1342–1346.

Hoffman, P.F., Halverson, G.P., Domack, E.W., Husson, J.M., Higgins, J.A., Schrag, D.P., 2007. Are basal Ediacaran (635 Ma) post-glacial "cap dolostones" diachronous? Earth and Planetary Science Letters 258, 114–131.

Hoffmann, K.-H., Condon, D.J., Bowring, S.A., Prave, A.R., Fallick, A., 2006. Lithostratigraphic Carbon (≙13C) Isotope and U–Pb Zircon Age Constraints on Early Neoproterozoic (ca. 755 Ma) Glaciation in the Gariep Belt southern Namibia Snowball Earth Conference July 16–21, 2006, Ascona, Switzerland [abstract] 51.

Jacobsen, S.B., Kaufman, A.J., 1999. The Sr, C and O isotopic evolution of Neoproterozoic seawater. Chemical Geology 161, 37–57.

Jaffrés, J.B.D., Shields, G.A., Wallmann, K., 2007. The oxygen isotope evolution of seawater: A critical review of a long-standing controversy and an improved geological water cycle model for the past 3.4 billion years. Earth-Science Reviews 83, 83–122.

James, N.P., Narbonne, G.M., Sherman, A.G., 1998. Molar-tooth carbonates: shallow subtidal facies of the Mid- to Late Proterozoic. Journal of Sedimentary Research 68, 716–722.

Kasting, J.F., Tasewell Howard, M., Wallmann, K., Veizer, J., Shields, G., Jaffres, J., 2006. Paleoclimates, ocean depth, and the oxygen isotopic composition of seawater. Earth and Planetary Science Letters 252, 82–93.

Kaufman, A.J., Knoll, A.H., 1995. Neoproterozoic variations in the carbon isotopic composition of seawater: stratigraphic and biogeochemical implications. Precambrian Research 73, 27–49.

Kaufman, A.J., Hayes, J.M., Knoll, A.H., Germs, G.J.B., 1991. Isotopic compositions of carbonates and organic carbon from upper Proterozoic successions in Namibia:

stratigraphic variation and the effects of diagenesis and metamorphism. Precambrian Research 49, 301–327.
Kaufman, A.J., Jacobsen, S.B., Knoll, A.H., 1993. The Vendian record of C- and Sr-isotopic variations: implications for tectonics and paleoclimate. Earth and Planetary Science Letters 120, 409–430.
Kaufman, A.J., Jiang, G., Christie-Blick, N., Banerjee, D.M., Ria, V., 2006. Stable isotope record of the terminal Neoproterozoic Krol platform in the Lesser Himalayas of northern India. Precambrian Research 147, 156–185.
Kazmin, V., 1972. The Geology of Ethiopia. Ethiopian Institute of Geological Surveys Note 821051-12, Addis Ababa, 208 p.
Kendall, B.S., Creaser, R.A., Selby, D., 2006. Re-Os geochronology of postglacial black shales in Australia: constraints on the timing of the 'Sturtian' glaciation. Geology 34, 729–732.
Kennedy, M.J., Christie-Blick, N., Sohl, L.E., 2001. Are proterozoic cap carbonates and isotopic excursions a record of gas hydrate destabilization following Earth's coldest intervals? Geology 29, 443–446.
Kirschvink, J.L., 1992. Late proterozoic low-latitude global-glaciation: the Snowball Earth. In: Schopf, J.W., Klein, C. (Eds.), The Proterozoic Biosphere. Cambridge University Press, Cambridge, UK, pp. 51–52.
Kitachew, W.T., 1974. Regional geological report of Axum Sheet (ND 37-6). Ethiopian Institute of Geological Surveys.
Knoll, A.H., 1992. Biological and biogeochemical preludes to the Ediacaran radiation. In: Lipps, J.H., Signor, P.W. (Eds.), Origin and Early Evolution of the Metazoa. Plenum, New York, pp. 53–84.
Knoll, A.H., Carroll, S.B., 1999. Early animal evolution: emerging views from comparative biology and geology. Science 284, 2130–2137.
Knoll, A.H., Hayes, J.M., Kaufman, A.J., Swett, K., Lambert, I.B., 1986. Secular variation in carbon isotope ratios from upper Proterozoic successions of Svalbard and East Greenland. Nature 321, 832–838.
Knoll, A.H., Kaufman, A.J., Grotzinger, J.P., Kolosov, P., 1995. Integrated approaches to terminal Proterozoic stratigraphy: an example from the Olenek Uplift, northern Siberia. Precambrian Research 73, 251–270.
Kröner, A., 2001. The Mozambique belt of East Africa and Madagascar: significance of zircon and Nd model ages for Rodinia and Gondwana supercontinent formation and dispersal. South African Journal of Geology 105, 151–167.
Malone, M.J., Baker, P.A., Burns, S.J., 1996. Hydrothermal dolomitization and recrystallization of dolomite breccias from the Miocene Monterey Formation, Tepusquet area, California. Journal of Sedimentary Research 66, 976–990.
Mazzullo, S.J., 2000. Organogenic dolomitization in peritidal to deep-sea sediments. Journal of Sedimentary Research 70, 10–23.
Meert, J.G., 2003. A synopsis of events related to the assembly of eastern Gondwana. Tectonophysics 362, 1–40.
Melezhik, V.A., Gorokhov, I.M., Kuznetsov, A.B., Fallick, A.E., 2001. Chemostratigraphy for Neoproterozoic carbonates: implications for 'blind dating'. Terra Nova 13, 1–11.
Miller, N.R., 1990. Utility of primary and secondary carbonates for strontium isotope chronostratigraphy of the Monterey formation, offshore Santa Barbara, California. AAPG Bulletin 74, 990.
Miller, N.R., 1995. Lithostratigraphic signal evaluation of the Miocene Monterey Formation, South Elwood Field, Santa Barbara-Ventura Basin, California. Ph.D. Dissertation. University of Texas at Dallas, 607 p.
Miller, N.R., Alene, M., Sacchi, R., Stern, R., Conti, A., Kröner, A., Zuppi, G., 2003. Significance of the Tambien Group (Tigre. N. Ethiopia) for Snowball Earth Events in the Arabian–Nubian Shield. Precambrian Research 121, 263–283.
Miller, N.R., Avigad, D., Stern, R.J., Beyth, M., Küster, D., Mehari, K., 2004a. The search for snowball Earth in the Arabian–Nubian Shield: reconnaissance geologic assessment of the Neoproterozoic Tsaliet and Tambien Groups in Northern Ethiopia. In: 20th Colloquium of African Geology, Orléans, France.
Miller, N.R., Avigad, D., Stern, R.J., Beyth, M., Küster, D., Gebresilassie, S., Mehari, K., 2004b. Of island arcs and icebergs? Strontium and carbon isotope stratigraphy of Ethiopian snowball Earth sequences. In: American Geophysical Union Fall Meeting 2004, PP33B-0943.
Miller, N.R., Schilman, B., Avigad, D., Stern, R.M., Beyth, M., 2006. Neoproterozoic snowball Earth—the Northern Ethiopian record. In: Snowball Earth Conference Proceedings, Ascona, Switzerland, 74–75 (abstract).
Misi, A., Veizer, J., 1998. Neoproterozoic carbonate sequence of the Una Group, Irecê Basin: chemostratigraphy, age and correlations. Precambrian Research 89, 87–100.
Narbonne, G.M., Kaufman, A.J., Knoll, A.H., 1994. Integrated chemostratigraphy and biostratigraphy of the upper Windermere Supergroup (Neoproterozoic), Mackenzie Mountains, northwestern Canada. Geological Society of America Bulletin 106, 1281–1291.
Nesbitt, H.W., Young, G.M., 1982. Early Proterozoic climates and plate motions inferred from major element geochemistry of lutites. Nature 299, 715–717.
Patchett, P.J., Chase, C.G., 2002. Role of transform continental margins in major crustal growth episodes. Geology 30, 39–42.
Pavlov, A.A., Hurtgen, M.T., Kasting, J.F., Arthur, M.A., 2003. Methane-rich Proterozoic atmosphere? Geology 31, 87–90.
Robb, L.J., Knoll, A.H., Plumb, K.A., Shields, G.A., Strauss, H., Veizer, J., 2004. The Precambrian: the Archean and Proterozoic Eons. In: Gradstein, F., Ogg, J., Smith, A.G. (Eds.), Geologic Time Scale. Cambridge University Press, Cambridge, pp. 129–140.
Schidlowski, M., 1987. Application of stable carbon isotopes to early biochemical evolution of earth. Annual Review of Earth and Planetary Science 15, 47–72.
Shackleton, N.J., 1974. Attainment of isotopic equilibrium between ocean water and the benthonic foraminifera genus Uvigerina: isotopic changes in the ocean during the last glacial. Colloques Internationaux du C.N.R.S. 219, 203–209.
Sheppard, S.M.F., Schwarcz, H.P., 1970. Fractionation of carbon and oxygen isotopes and magnesium between metamorphic calcite and dolomite. Contributions to Mineralogy and Petrology 26, 161–198.
Shields, G., 2002. 'Molar-tooth microspar': a chemical explanation for its disappearance ~750 Ma. Terra Nova 14, 108–113.
Sifeta, K., Roser, B.P., Kimura, J.I., 2005. Geochemistry, provenance, and tectonic setting of Neoproterozoic metavolcanic and metasedimentary units, Werri area, Northern Ethiopia. Journal of African Earth Sciences 41, 212–234.
Stern, R.J., 1994. Arc assembly and continental collision in the Neoproterozoic East African Orogen: implications for the consolidation of Gondwanaland. Annual Reviews of Earth and Planetary Sciences 22, 319–351.
Stern, R.J., Abdelsalam, M.G., Schandelmeier, H., Sultan, M., Wickham, S., 1993. Carbonates of the Keraf Zone, NE Sudan; a Neoproterozoic (ca. 750 Ma) passive margin on the eastern flank of West Gondwanaland? In: Geological Society of America Annual Meeting, Abstracts with Programs 25, A49.
Stern, R.J., Avigad, D., Miller, N.R., Beyth, M., 2006. Geological Society of Africa Presidential Review: evidence for the Snowball Earth Hypothesis in the Arabian–Nubian Shield and the East African Orogen. Journal of African Earth Sciences 44, 1–20.
Tadesse, T., 1997. The Geology of Axum Area (ND 37-6). Ethiopian Institute of Geological Surveys, Addis Ababa. (Memoir No. 9), 184 p.
Tadesse, T., 1999. Axum sheet geological map. Geological Survey of Ethiopia, Addis Ababa, Ethiopia. 1:250,000 map.
Tadesse, T., Hoshino, M., Sawada, Y., 1999. Geochemistry of low-grade metavolcanic rocks from the Pan-African of the Axum area, northern Ethiopia. Precambrian Research 99, 101–124.
Tadesse, T., Hoshino, M., Suzuki, K., Iizumi, S., 2000. Sm–Nd, Rb–Sr and Th–U–Pb zircon ages of syn- and post-tectonic granitoids from the Axum area of northern Ethiopia. Journal of African Earth Sciences 30, 313–327.
Teklay, M., Kröner, A., Metzger, K., 2001. Geochemistry, geochronology and isotope geology of Nakfa intrusive rocks, northern Eritrea: products of a tectonically thickened Neoproterozoic arc crust. Journal of African Earth Sciences 33, 283–301.
Tsige, L., Abdelsalam, M.G., 2005. Neoproterozoic-early Paleozoic gravitational tectonic collapse in the southern part of the Arabian–Nubian Shield: the Bulbul Belt of southern Ethiopia. Precambrian Research 38, 297–318.
Tucker, M.E., 1983. Diagenesis, geochemistry, and origin of a Precambrian dolomite: The Beck Spring Dolomite of eastern California. Journal of Sedimentary Petrology 53, 1097–1119.
Tucker, M.E., 1985. Calcitized aragonite ooids and cements from the late Precambrian Biri Formation of southern Norway. Sedimentary Geology 43, 67–84.
Vail, J.R., 1983. Pan-African crustal accretion in northeast Africa. Journal of African Earth Science 1, 285–294.
Wright, D.T., Oren, A., 2005. Nonphotosynthetic bacteria and the formation of carbonates and evaporites through time. Geomicrobiology Journal 22, 27–53.